Three-dimensional structure of sub-mesoscale eddies on the continental shelf

Liliane Paranhos Bitencourt[1], Charitha Pattiaratchi[1], Simone Cosoli[1], Yasha Hetzel[1]

School of Engineering & the UWA Oceans Institute, the University of Western Australia, Perth, 6009, Australia.

Correspondence to: Charitha Pattiaratchi (chari.pattiaratchi@uwa.edu.au)

Abstract. Sub-mesoscale eddies are oceanic features crucial for energy transfer processes, transport of heat and biogeochemical tracers, and for promoting diversity in marine ecosystems. Their relatively small length scales (<20 km) and short lifespans ~O(days), make their characterization challenging using field measurements. In this paper, we combined remote sensing, ocean glider, High-Frequency Radar, shipborne, and mooring data to investigate the internal structure and dynamical properties of sub-mesoscale eddies and peddies ('petite' eddies; diameters ≤10 km extending through the water column) along the Wadjemup (Rottnest) Continental Shelf (WCS), Western Australia. Data collected in August 2010 showed an anti-cyclonic (counterclockwise) mesoscale eddy spawning several cyclonic (clockwise), cold core sub-mesoscale eddies that promoted upwelling (vertical extension of 185m) with maxima in chlorophyll concentration at the centre. Results suggested that sub-mesoscale eddies drive chlorophyll advection either at (in) their periphery (centre) of cyclonic (anti-cyclonic) eddies, or at their interfaces. In general, cyclonic eddies promoted upwelling and anti-cyclonic eddies promoted downwelling; however, our data also showed that upwelling conditions could also occur in anti-cyclonic eddies. Winds were found to affect the internal structure and lifecycle of sub-mesoscale eddies, particularly under strong wind (speeds > 7 m s^{-1}) conditions, through upwelling and/or vertical mixing. In the presence of dense shelf water outflows along the continental shelf, sub-mesoscale eddies were found to trap, upwell, and transport denser nearshore waters off the continental shelf. This unique dataset provided a detailed picture of the three-dimensional structure of sub-mesoscale eddies, including the characterization of sub-surface eddies, and contributes to the understanding of their role in chlorophyll advection in shelf and coastal environments.

1 Introduction

Mesoscale and sub-mesoscale features are ubiquitous in the world's oceans, acting as reservoirs and pathways of 90% of the ocean's kinetic energy (Carpet et al., 2008; Chelton et al., 2007; Ferrari and Wunsch, 2009; Fu et al., 2010). They are crucial for maintaining energy balance across scales (Chen et al., 2023) and transporting heat, momentum, mass, and biogeochemical tracers in the oceans, also promoting biodiversity in marine ecosystems (Damien et al., 2023; Levy et al., 2018; Mahadevan, 2016). In continental shelf regions, these processes also facilitate exchanges between offshore and coastal waters. Through cross-shore transport, they contribute to carbon export and the fate of particulate organic carbon and biogeochemical budgets (Mahadevan, 2014) with important implications for plankton, fisheries, and fisheries management (Akpinar et al., 2020; 2022; Guerrero et al., 2019; Irigoien et al., 2007). Sub-mesoscale eddies contribute to nutrient cycling, primary production, structure and functioning of phytoplankton ecosystems in coastal areas (Fig. 1a; Lévy et al., 2001; Davila et al., 2021; Mahadevan and Tandon, 2016; Oguz et al., 2015; Veatch et al., 2024).

These features occur in the transition between mesoscale dynamics and small-scale turbulence (Thomas et al., 2008; Kubryakov et al., 2022). Sub-mesoscale processes are typically characterised by horizontal scales of order 1–20 km, although their spatial extent is not universal and depends strongly on the local Rossby deformation radius and stratification. Their temporal scales generally range from hours to a few days. Their strong ageostrophic nature can lead to Rossby numbers ~O(1) or larger and induce high vertical velocities in their core (10-100 m day^{-1}; Lévy et al., 2012; McWilliams, 2016; Thomas et al., 2008; Zatsepin et al., 2019).

Consequently, they can lead to intense localised mixing (McWilliams, 2016; Thomas et al., 2008) and vertical transport of nutrients and suspended matter (Rubio et al., 2018; Su et al., 2018; Zhang and Qiu, 2020), driving phytoplankton growth and enhancing primary productivity or reducing biological production in the euphotic zone through advection, upwelling or downwelling (Davila et al., 2021; Lévy et al., 2012; Mahadevan and Tandon, 2016; Thomas et al., 2008).

Understanding the impacts of small and short-lived features on ecosystems is crucial but limited due to technical challenges, such as the availability of data with sufficient spatial and temporal resolution (Liu et al., 2015; Parks et al., 2009; Zhang et al., 2019). Remote sensing observations stand out as powerful tools for detecting and tracking sub-mesoscale features (e.g., Bitencourt et al., 2025; Cosoli et al., 2020; Lipinskaya et al., 2023; Zatsepin et al., 2019).

However, the data is limited to the surface and insufficient for characterising their internal structure. More conventional in situ measurements offer detailed, high-resolution vertical profiles that can help to resolve internal dynamics; however, not with sufficient resolution. Thus, a combination of datasets (e.g., vessels, moorings, ocean gliders, autonomous underwater vehicles, satellite) can provide a detailed picture of the three-dimensional structure of eddies and their evolution in coastal, shelf and offshore environments (e.g., Bouffard et al., 2012; Bosse et al., 2017; Fayman et al., 2019; Veatch et al., 2024).

The Wadjemup (Rottnest) Continental Shelf (WCS), a microtidal and oligotrophic marine environment located on the south-west coast of Australia, is a region rich in sub-mesoscale eddies (Fig. 1a; Bitencourt et al., 2025; Cosoli et al., 2020; Kendrick et al., 2023; Pattiaratchi and Eliot, 2009). In this region, the Australian Integrated Marine Observing System (IMOS) has been collecting data from different platforms for over a decade and enabled the characterisation of small-to-large scale features (e.g., Bitencourt et al., 2024; 2025; Cosoli et al., 2020; Kodithuwakku et al., 2024; Pattiaratchi et al., 2017).

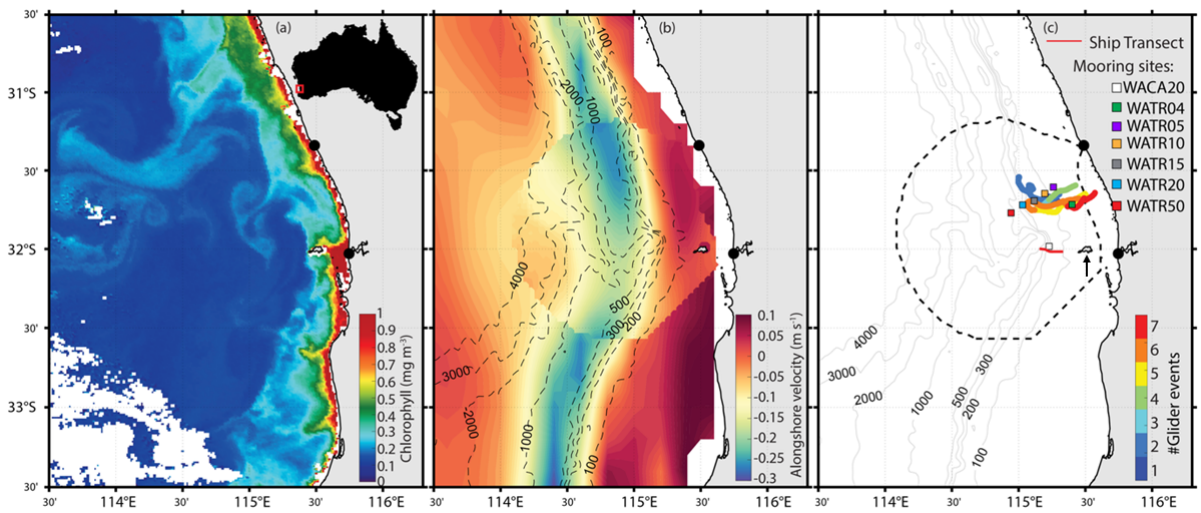

Figure 1. (a) Remotely sensed chlorophyll-a on 28 March 2016, (b) long-term (2010-2018) averaged alongshore velocities from altimetry and HFR observations in Wadjemup Continental Shelf; and (c) HFR domain (dashed line), glider (coloured lines) and ship (red line) tracking, and mooring locations (coloured squares). Bathymetric contours (in metres) are shown in (b,c). Black dots at the shoreline in (a,b,c) represent HFR shore stations. The upward arrow in (c) points to Rottnest Island the location of the wind records

Complex circulation patterns across multiple scales characterise the WCS area, such as an anomalous poleward eastern boundary current, micro-tidal regime, wind-driven coastal circulation, sub- to meso-scale eddies, complex bathymetric features with a canyon reaching

as deep as 4000m, and circulation responses to remote forcing associated with the Leeuwin Current system and coastally trapped waves. Wind forcing is amongst the strongest globally and drives the circulation along the shelf (Bitencourt et al., 2024; Mihanović et al, 2016), particularly under the summer land-sea breeze regime (maximum daily wind speeds frequently exceeding 15 ms^{-1}) and winter storms (speeds > 30 m s^{-1}; Pattiaratchi et al., 1997; Rafiq et al., 2020; Verspecht and Pattiaratchi, 2010; Zaker et al., 2007). Strong inertial-diurnal resonance also occurs in the region due to its proximity to the critical latitude (30°S) (Mihanović et al., 2016; Rafiq et al., 2020). In addition, strong air-sea heat fluxes and low river outflows along the coast contribute to dense shelf water transport which is then transported offshore as gravity currents (Mahjabin et al., 2019a,b; Pattiaratchi et al., 2011).

The Leeuwin Current (LC), Capes Current (CC), wind forcing, their interactions and deeper water dynamics control the circulation along the South-west Australian coast (Pattiaratchi and Woo, 2009; Wijeratne et al., 2018; Woo and Pattiaratchi, 2008). The LC is a warm, relatively shallow (<300 m depth) and narrow (~100 km width) eastern boundary current that flows poleward against the prevailing equatorward winds favouring downwelling along the shelf break towards the South Australian coast (Feng et al., 2009; Pattiaratchi and Woo, 2009; Pearce and Pattiaratchi, 1999; Wijeratne et al., 2018). Thus, the LC, that inhibits large-scale upwelling, contrasts with the equatorward-flowing upwelling-favourable currents typically found along the eastern boundaries of ocean basins. In contrast, the CC is a seasonal inner-shelf wind-driven equatorward-flowing current that promotes weak, shallow (<50 m) upwelling of more saline and colder water (21-24°C) inshore of LC (Bitencourt et al., 2024; Gersbach et al. 1999; Pattiaratchi and Woo, 2009; Pearce and Pattiaratchi, 1999).

Local and large-scale wind patterns favour, reinforce or weaken the poleward-flowing LC and the seasonal wind-driven equatorward-flowing CC (Fig.1b). Under prevailing southerly winds in the warmer months, CC flows equatorward along the inner shelf, whilst the LC weakens and is displaced offshore (Bitencourt et al., 2024; Gersbach et al., 1999; Pearce and Pattiaratchi, 1999). Under weaker southerly or variable winds, particularly over cooler months, CC is absent whilst the LC is strongest along the shelf (Bitencourt et al., 2024; Cresswell, 1996; Pattiaratchi and Woo, 2009; Wijeratne et al., 2018).

Mesoscale and sub-mesoscale eddies are ubiquitous features in the region, particularly along the interfaces of the LC (Bitencourt et al., 2024; 2025; He et al., 2021; Kodithuwakku et al., 2024; Rennie et al., 2007). They spawn along the LC path, particularly through interactions with coastal and bottom topography (changes in coastline orientation, bathymetric features;

Cosoli et al., 2020; Kodithuwakku 2024; Rennie et al., 2007; Waite et al., 2007), barotropic instabilities and interactions with the CC and offshore mesoscale eddies (Bitencourt et al., 2024; 2025; Pattiaratchi and Mihanović, 2014). Peddies are defined as sub-mesoscale eddies that form in shallow coastal waters, typically in water depths <200 m and occupy the majority of the water column. They have typical eddy diameters <10 km and lifespans of 1-2 days. They are generated in regions of strong horizonal flow shear and influenced by bottom topography and friction because their vertical extent often spans much of the water column. Sub-mesoscale eddies and peddies are difficult to observe and characterize due to their small spatial and temporal scales, with limitations in both observational capabilities and modelling resolution hindering a complete understanding of their internal structure and variability under different forcing condition (Bitencourt et al., 2025; Cosoli et al., 2020; Pattiaratchi and Mihanović, 2014).

In this paper, we use a multi-platform approach to investigate the internal structure of sub-mesoscale eddies (<20km diameter) and peddies (i.e., 'petite' eddies; diameters ≤10 km extending through the water column) along the Wadjemup (Rottnest) Continental Shelf. In particular, we aim to: (1) characterize their physical and biogeochemical structure and determine whether these features display consistent signatures across observations; and (2) evaluate how these eddies influence chlorophyll distribution on the shelf.

2 Data and Methods

The Australian Integrated Marine Observing System (IMOS) was established in 2006 and this study used data acquired as part of IMOS in Western Australia (WAIMOS) using a variety of data collecting platforms including research vessels, oceanographic mooring time series, ocean gliders, surface currents using High Frequency Radar, satellite remote sensing and meteorological data.

2.1 R/V Southern Surveyor

The R/V *Southern Surveyor* research cruise (SS2010_v06) collected hydrographic and biological data between 29 July to 09 August 2010, with the aim of investigating the slope and shelf processes along the south-west region of Western Australia in winter (Pattiaratchi and Hanson, 2010). Data collected included that from a towed platform Nacelle with profiles from the surface to a maximum depth of 200m in a yo-yo mode at a vertical resolution of 1 m. The horizontal spacing of each dive varied within 1–4 km, depending on the velocity of the ship.

Sensors on Nacelle included a Seabird SBE911 CTD, a SBE43 oxygen sensor, a Chelsea Aqua tracker Fluorometer (N-Chl, Table 1), and a Wetlabs C-Star™ transmissometer. Sensor calibrations were undertaken using bottle samples (Pattiaratchi and Hanson, 2010).

Current profiles were collected using a hull-mounted, 75kHz RDI Acoustic Doppler Current Profiling (ADCP), collecting subsurface current data at a 10 min ensemble time and a vertical resolution of 16 m. Data were collected by the Commonwealth Scientific and Industrial Research Organisation (CSIRO). A transect (Fig. 1c) showed the presence of a peddie on 3 August 2010, west of Rottnest Island.

2.2 Moorings

Subsurface currents, temperature, salinity, chlorophyll fluorescence (M-Chl) data were collected across several mooring locations within the WCS (Fig. 1c). Moorings were located between 45-65 km offshore, at nominal water depths of 40m, 50m, 100m, 150m, 200m and 500m (mooring codes: WATR04, WATR05, WATR10, WATR15, WATR20 and WATR50, respectively), and in the Perth Canyon (WACA20) at a depth of ~200 m. They were equipped multiparameter probes with SBE39 and SBE39plus sensors from SeaBird Electronics and RBR XR420-CTD from RBR. Bottom-mounted, upward-looking acoustic 190 kHz Doppler current meter from Nortek Continental measured horizontal and vertical currents along the water column (see Mihanović et al., 2016; Mahjabin et al., 2019b). At the WACA20 mooring site (Fig. 1c), a Wetlabs Water Quality Meter (WQM) was deployed at 75m water depth that measured, temperature, salinity and chlorophyll fluorescence (M-Chl, Table 1). Further information regarding data processing and quality control procedures in WCS-IMOS mooring data refer to Morello et al. (2014) and Bui and Feng (2025).

2.3 Ocean gliders

High-resolution sub-surface measurements of salinity, temperature, dissolved oxygen (DO) and chlorophyll fluorescence (G-Chl, Table 1) were collected using Teledyne Webb Research Slocum electric G2 gliders sampling to a maximum 200 m water depth. Each glider was equipped with a pumped SeaBird Scientific CTD sensor, WETLabs BBFL2SLO 3 parameter optical sensor (Chlorophyll fluorescence G-Chl, coloured dissolved organic matter, and 660 nm backscatter), and an Aanderaa Oxygen optode (Pattiaratchi et al., 2017; Mahjabin et al., 2019b). The glider collected science data (CTD_bio-optics) between the surface to a maximum 200 m depth with a mean travel speed of ~25 km day^{-1} (Pattiaratchi et al., 2011). Data sampling rate was set at 4 Hz, resulting in measurements with approximately 7 cm vertical

resolution. The gliders were programmed to surface every 2 hours and transmit its position and send a subset of science data to the shore station. Over this 2-hour period the glider traversed 1-2 km, performing vertical 5-10 vertical dives, resulting in the lateral spacing of profiles between 100-250 m in 50 m and 200 m water depths, respectively. Data were post-processed after recovery with QA/QC procedures as described in Woo (2021). The science data were processed using the IMOS ocean glider analysis software *Gliderscope* (https://imos.org.au/data/ocean-informationresources/gliderscope-software) in MATLAB (Hanson et al., 2017). The data were linearly interpolated into bins of 0.2 m vertically and 4.3 min in time into a 1000x1000 grid using *Gliderscope* (Hanson et al., 2017). The calibration in temperature and salinity measurements achieved an accuracy of ±0.002°C and ±0.01, respectively (Chen et al., 2019). All the sensors on the gliders were returned to the manufacturer for calibration annually. This included the CTD, DO Optode and the Ecopuck (Thomson et al., 2026). Depth-averaged current (DAC) from the Slocum glider was estimated as the difference between GPS-derived displacement over a dive cycle and the glider's dead-reckoned displacement based on its hydrodynamic flight model, divided by the elapsed time (Rudnick et al., 2004). These techniques are included in the routines provided by the manufacture. There was no vertical averaging (they are depth mean currents) or smoothing applied (have a value every surfacing in our case every 2 hours). The quality control was only to check the values of derived velocities are within an acceptable range. The glider derived DAC speeds were within the range $0 < DAC < 0.55$ m s^{-1}.

For our analysis, we selected events from seven different glider missions (Fig. 1c; Table 2): (1) 03-04 August 2010; (2) 16-18 August 2010; (3) 16 February 2014; (4) 23 February 2014; (5) 26-27 May 2015; (6) 28-30 May 2015; and (7) 01-02 June 2015.

2.4 High-Frequency Radar

High-resolution (4x4 km; 1 hour) surface current fields (top ~1.5m layer) were collected with a pair of WEllen Radar (WERA) phased-array High-Frequency Radar (HFR) shore-based stations (Fig. 1c) located at Guilderton (GUI) and Fremantle (FRE). In this study, we used quality-controlled, delayed-mode, 2x2 km interpolated gridded, 33 h low-pass filtered, hourly and daily averaged surface current data (Bitencourt et al., 2024; Cosoli and Grcic, 2024) during selected events identified from the ocean glider data between 2010-2015 (see above and Table 2). Full descriptions of the instrumentation, specifications used in the WCS – HFR system and quality control tests are provided in Mihanović et al. (2016), Bitencourt et al. (2024; 2025), Cosoli and Grcic (2024) and Cosoli et al. (2018; 2020).

2.5 Ocean colour data

Level 3 daily sea surface chlorophyll concentration data (SCC, 1 km resolution, Table 1) and Sea Surface Temperature skin (SST, ~2 km resolution) were available from MODIS Aqua and Advanced Very High-Resolution Radiometer (AVHRR) and were accessed through IMOS (Govekar et al., 2022).

2.6 Wind data

Hourly wind speed and direction at Rottnest Island weather station (located ~25km offshore from the coast, 43m elevation, Figure 1c) were obtained from the Bureau of Meteorology (BOM). Wind speeds were converted to the standard 10m reference height (van der Mheen et al., 2020).

2.7 Analysis techniques

To characterize the vertical structure and dynamical properties of submesoscale eddies and peddies, we estimated relative vorticity and Rossby number using velocity measurements from different observational platforms. Our main objective was not to derive a complete two-dimensional vorticity field, but rather to obtain an order-of-magnitude estimate of the Rossby number (i.e., whether R_o was O(0.1), O(1), or larger) in order to assess whether the observed structures were consistent with sub-mesoscale dynamics. Because the available observations differed substantially in their spatial sampling, different methodological approaches and approximations were required for each dataset, particularly for the glider and shipborne measurements where only partial velocity information was available.

In the following equations, u and v represent the zonal and meridional velocity components of ocean currents, respectively. U is the velocity component perpendicular to the glider track, s is the distance along the perpendicular glider track, and ζ is the relative vorticity. The Coriolis parameter is defined as $f = 2\Omega\sin\ \theta$, where $\Omega = 2\pi/86400$ rad s^{-1} is the Earth's rotation rate and θ is the latitude.

For the HFR observations, the availability of gridded two-dimensional surface velocity fields allowed the direct calculation of relative vorticity as $\zeta = \frac{\partial v}{\partial x} - \frac{\partial u}{\partial y}$, using a central finite-difference scheme (Bitencourt et al., 2025; Cosoli et al., 2020). The Rossby number was then estimated as $R_o = \frac{\zeta}{|f|}$.

The moored ADCP observations were mainly used to investigate the temporal variability and vertical structure of the observed features, rather than to estimate horizontal vorticity, since the fixed-point measurements do not resolve horizontal velocity gradients.

For the glider and shipborne ADCP observations, the spatial sampling did not allow reconstruction of the full two-dimensional velocity field. Therefore, relative vorticity could not be directly estimated in a dynamically rigorous sense (e.g., from cylindrical eddy geometry and azimuthal velocity structure). Instead, we used along-track horizontal shear as a proxy to obtain an order-of-magnitude estimate of Rossby number following Rossi et al. (2013).

Depending on the orientation of the transect relative to the observed structure, either the zonal shear component $(\partial v/\partial x)$ or the meridional shear component $(-\partial u/\partial y)$ was estimated. For the glider observations, the Rossby number proxy was calculated as $R_o = \frac{\partial U/\partial s}{|f|}$. For the shipborne ADCP observations collected on 3 August 2010 (Fig. 1c), we applied the zonal shear approximation $R_o = \frac{\partial v/\partial x}{|f|}$ was applied due to the predominantly east–west orientation of the ship transect.

Because these estimates rely on a single velocity component, they likely underestimate the magnitude of the full relative vorticity field. However, assuming approximate rotational symmetry of the observed structures, the along-track shear measurements still provide a useful qualitative estimate of circulation strength and Rossby number. Their primary purpose is to assess whether the observed structures exhibit Rossby numbers of order unity, consistent with submesoscale dynamics.

Different approaches were also used to estimate the horizontal dimensions of the sub-mesoscale eddies and peddies. For the gridded HFR data, an eddy-detection algorithm (Nencioli et al., 2010) was applied to extract ellipse characteristics, including the major and minor axes and eccentricity (see Bitencourt et al., 2025; Cosoli et al., 2020). For the glider observations, two methods were applied on a case-by-case basis: (1) fitting an ellipse to looping glider trajectories in cases where the platform appeared temporarily trapped and advected within the eddy core, providing an approximate estimate of the horizontal scale of the structure, and (2) defining the horizontal extent of the surface temperature anomaly.

2.8 Chlorophyll measurements

The study area is an oligotrophic region, with low chlorophyll concentration (<1 mg m^{-3}; Chen et al., 2019). Chlorophyll was measured using multiple observational platforms and

sensors, including satellite remote sensing (SCC) and in situ chlorophyll fluorescence (Table 1). This study focuses on relative changes in chlorophyll concentration near sub-mesoscale eddies and peddies rather than absolute values. Data sources are identified by acronyms corresponding to each platform and sensor (Table 1).

Table 1 – Summary of chlorophyll measurements.

Platform	**Sensor**	**Depth**	**Calibration (reference)**	**Acronym**
Satellite	Modis Aqua	~1-10 m	OC3 model (O'Reilly and Werdell, 2019)	SCC
Nacelle (ship)	Chelsea Aqua tracker Fluorometer	250 m	HPLC discrete samples (Earp et al. 2011)	N-Chl
Mooring	Wetlabs Water Quality Meter (WQM)	75 m	computed from fluorometer sensor raw counts measurements (Earp et al. 2011)	M-Chl
Ocean Glider	WETLabs BBFL2SLO 3	200 m	IMOS ocean glider facility (Thomson et al. 2026)	G-Chl

Table 2 - Wind forcing conditions and eddy properties during selected events.

	Eddy Number	Date	Wind Speed ($m\ s^{-1}$)	Wind Direction	Platform	Eddy Radius (km)	Rotation Sense	Ro	Vertical uplift (m)
Event 1	**#1**	02 August 2010	6.7 – 8.2	N	HFR, mooring	8	C	4.1	185
		03 August 2010	2.1 – 3.6	S	HFR, mooring, ship	8	C	4.1	185
	#2	16–19 August 2010	3.1 – 15.9	S, SE	HFR, ocean glider	3	C	15	120
	#3					2		10	100
Event 2	**#4**	16–21 April 2010	3.1 – 7.7	S, SE	HFR, mooring	24	C	0.5	80
	#5					8	AC	0.4	100
	#6					8	AC	0.6	45
	#7					15	C	0.5	80
	#8					21 / 8	C	0.6	130
	#9					24	AC	0.3	50
	#10					28	AC	0.8	-
Event 3	**#11**	16 February 2014	11.3 – 12.8	S, SE	HFR	8	AC	0.5	90
			6.2 – 11.3		Ocean glider	1		10	50
	#12	23 February 2014	8.7	S	HFR, ocean glider	3.5	C	0.5	50
Event 4	**#13**	26-27 May 2015	3.6	SE	HFR, ocean glider	1	C	5	45
	#14	28-30 May 2015	4.1 – 8.7	E, SE, S	HFR, ocean glider	5	C	5	175
	#15					1	C	10	50
	#16	01-02 June 2015	11.3 – 14.4	N, NW	HFR, ocean glider	2	C	5	25
	#17					2	C	15	30
	#18					1	C	15	30

3 Results

In this section, we present field measurements of 4 separate event periods detected using the different platforms in austral summer, autumn and winter (Table 2). The events included 18 different eddies with diameters 1- 28 km with maximum Rossby number >5 and a range of wind speeds.

3.1 Event 1 (shipborne/ocean glider): Mesoscale eddy and its peddies (August 2010)

Low SCC (0.3-0.4 mg m^{-3}), warm core (~21°C) anti-cyclonic (counterclockwise) mesoscale eddy (>20 km diameter) was present in the region over the period 2-4 August 2010 with centre at ~114°59'E and ~32°S (Fig. 2). Several cold core sub-mesoscale eddies and peddies can be clearly identified from the remotely sensed data either onshore or offshore in the south-west corner of the radar domain (Table 2).

A cold core peddie (eddy #1, 8 km radius, Table 2; Figs. 2 b,c,e,f) appeared between August 02-04, 2010, to the west of Rottnest Island and migrated westwards before dissipating. A transect by R/V *Southern Surveyor* using the profiling towed body Nacelle crossed this feature on August 03 revealing a slanted cone ("distorted vertical cone"; Fig. 3b) shape in the vertical distribution of N-Chl that appeared to follow the local bathymetry. The N-Chl peaked at ~0.7 mg m^{-3} below the surface with low concentrations below ~75 m depth along the shelf and ~150 m at deeper waters (Fig. 3b). Signatures of higher salinity, lower temperature, higher oxygenated water extending from ~150 m depth towards the surface could be also seen from ship transect data (Figs. 3c-e). The vertical distribution of subsurface currents showed the signature of a cyclonic feature with westward (northward) flow offshore and eastward (southward) flow at the inner shelf. The peddie was also characterised by a relatively high Rossby number ($|R_o|$~4.1; Figs. 3f-h).

Similar features were observed in the mooring data (Figs. 4a,b): lower M-Chl (~0.2 mg m^{-3}) and slight increase in salinity (Figs. 2a, 4a), vertical uplift of colder water and cross-shore flow reversal (from east to west orientation) on August 2, 2010 (Figs. 4b-d). These features were consistent with upwelling at the centre of the peddie. Between 2-3 August, M-Chl concentrations reached 1 mg m^{-3} at the mooring location (Fig. 4a). The peddie on August 3 was characterised by colder water uplifting from 185 m to 40 m depth, with a slight decrease in bottom M-Chl (<0.5 mg m^{-3}; Fig. 4a) and eastward (northward) flows (Figs. 4b-d). The slight

decrease in bottom M-Chl values during August 3 was associated with increased M-Chl levels at the surface which was also consistent with peddie-induced upwelling (Figs. 2b,d, 3, 4).

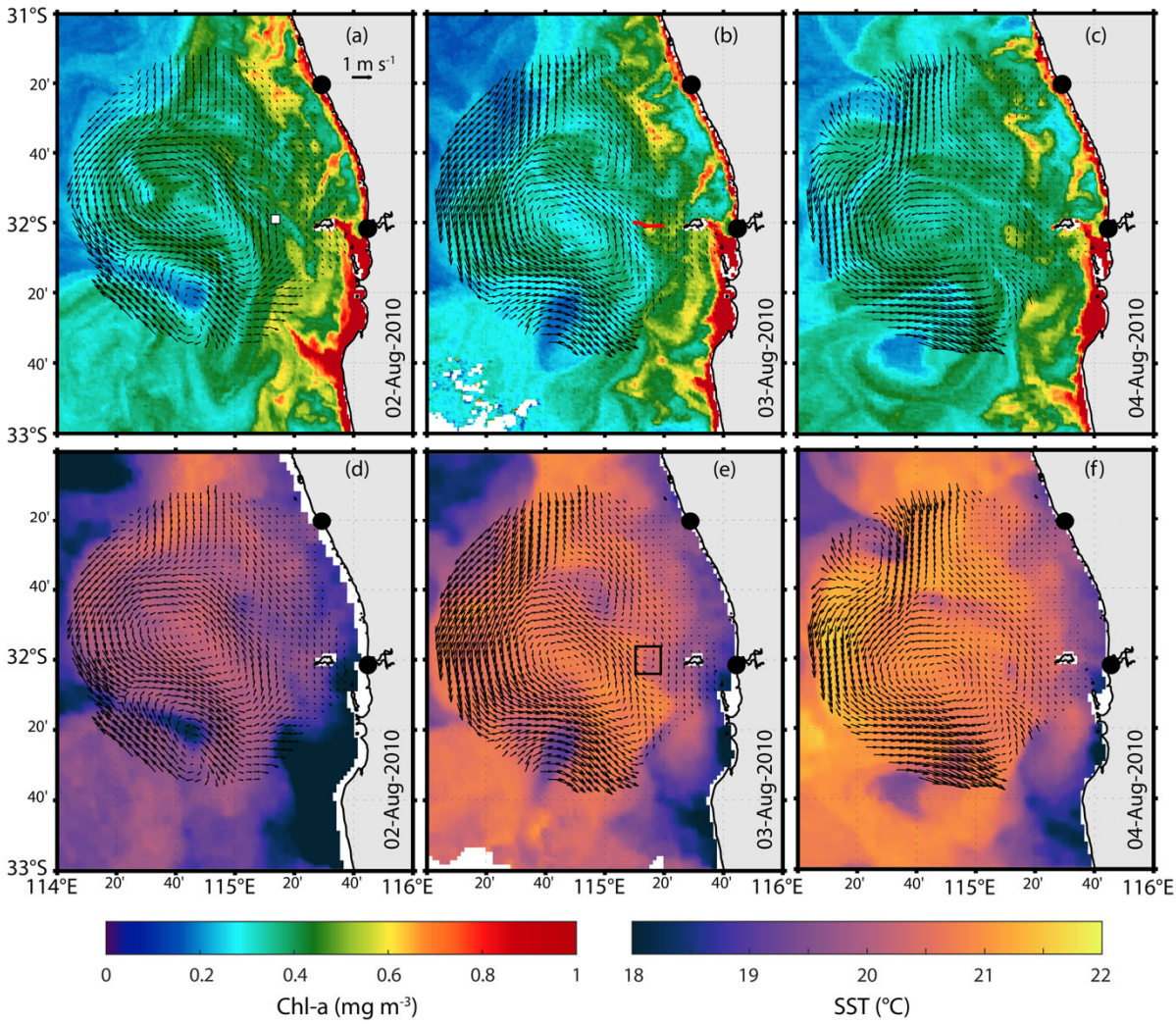

Figure 2. Remotely sensed (a-c) SSC, (d-f) Sea Surface Temperature and HFR surface currents (vectors) on 2-4 August 2010 (eddy #1, Event #1). The black dots represent HFR shore stations and the black-white square in (a) represents WACA20 mooring location (Fig. 1c). Red solid line in (b) is a ship transect on 3 August, and the black square in (e) represents the peddie location (eddy #1).

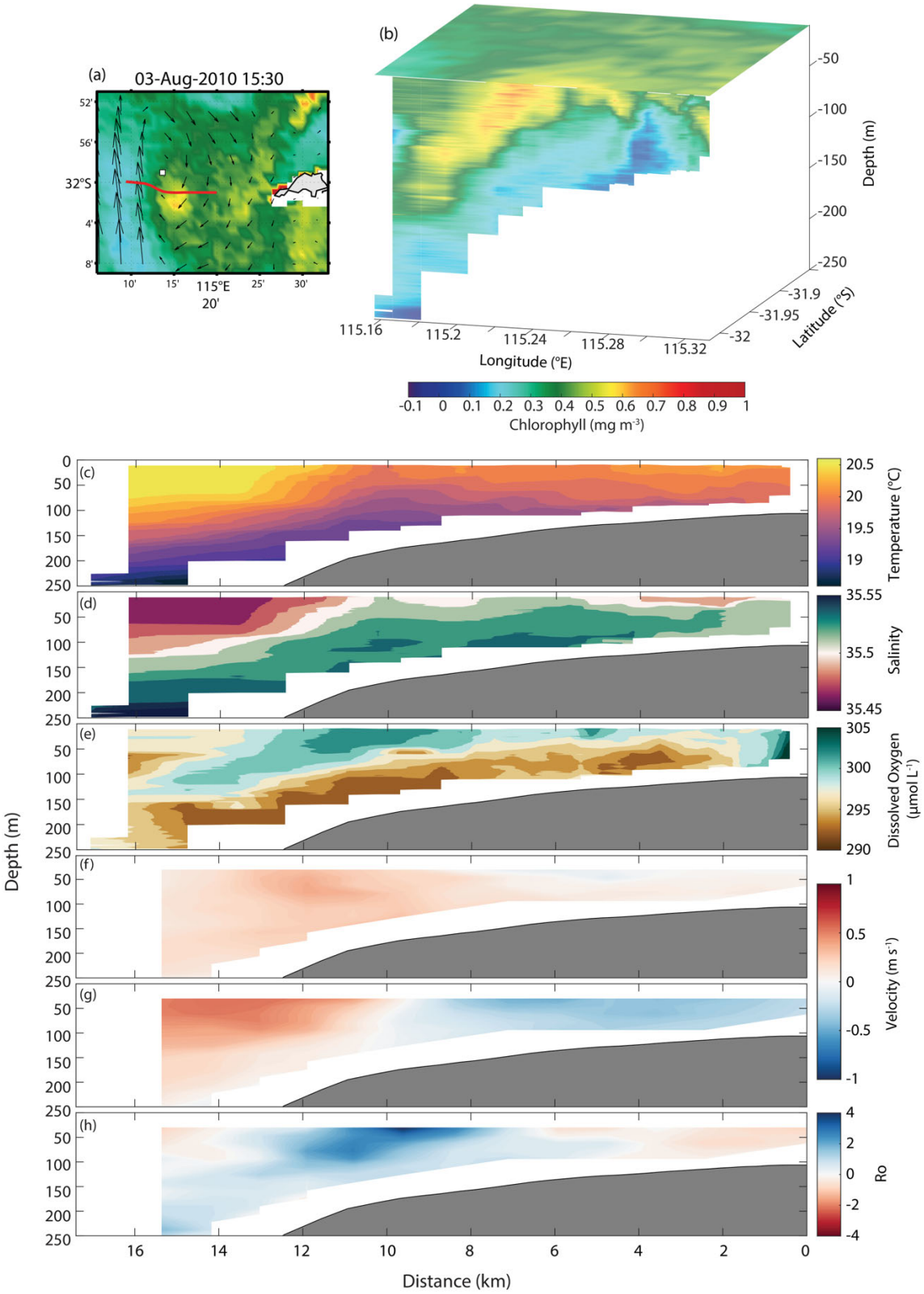

Figure 3. (a) SCC; (b) merged 3D structure of SCC (surface) and ship-based measurements N-Chl (subsurface), and (c-h) ship-based measurements of (c) temperature, (d) salinity, (e) dissolved oxygen, (f) u current component, (g) v current component, and (h) Rossby number on 3 August 2010 (eddy #1, Event #1). Red solid line in (a) is the ship-based transect shown in (b-h). Black-white square in (a) represents the WACA20 mooring location.

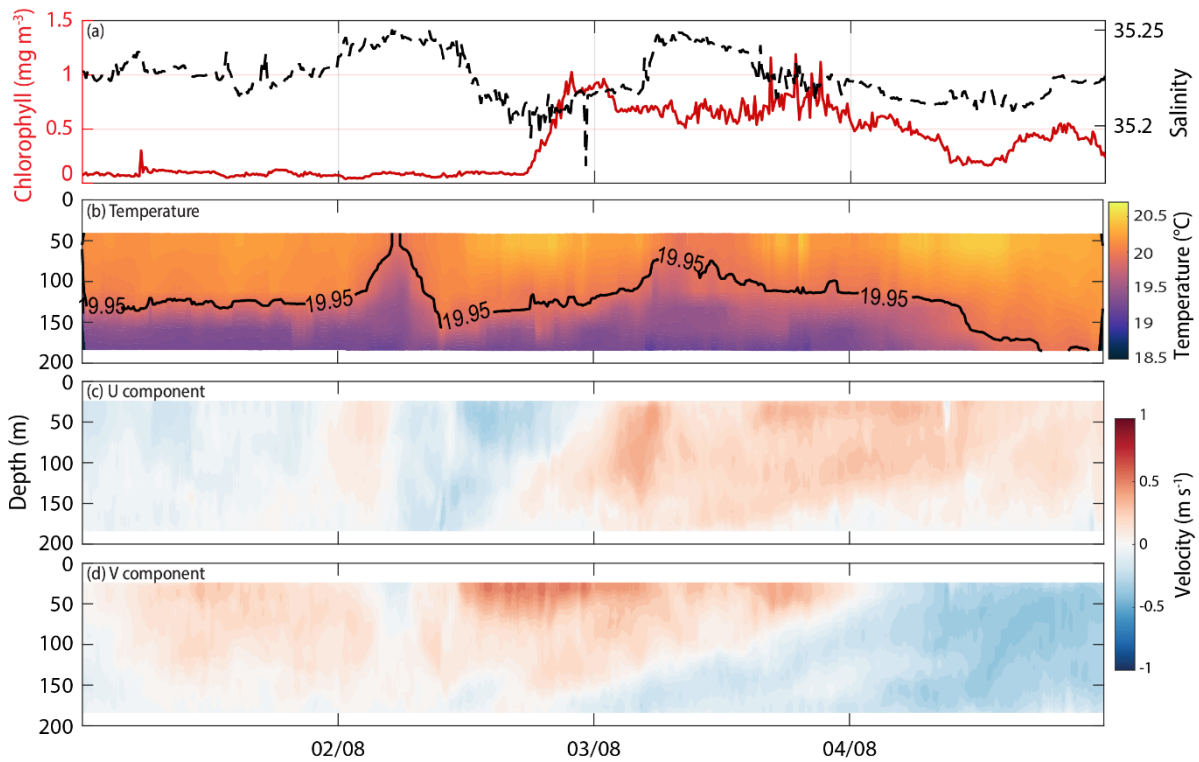

Figure 4. Mooring observations at WACA20 (Figs. 1c, 2a) in 01-04 August 2010 (eddy #1, Event #1) for (a) timeseries of M-Chl and salinity at 75m depth, (b) temperature, (c) u component, and (d) v component.

Later in the same month (between 16-19 August), an ocean glider intersected and then was entrained into two rapid rotating (speed > 1 m s^{-1}; eddies #2 and #3; radius ~2 km; Table 2) peddies. These peddies formed in the periphery of a sub-mesoscale eddy entraining colder and higher SCC closer to the coast (Figs. 5a,b). The peddies had a high Rossby number with $|R_o|>10$ and reached maximum DAC of 0.52 m s^{-1} and 0.51 m s^{-1} during the loops on 17 and 18 August, respectively (Fig. 5b). The uplift of colder (19.3°C), higher salinity (34.45), low G-Chl and DO (0.4 mg m^{-3}, 210 μM/l) water was detected in the cross-sectional vertical profiles (Figs. 5c,d,e).

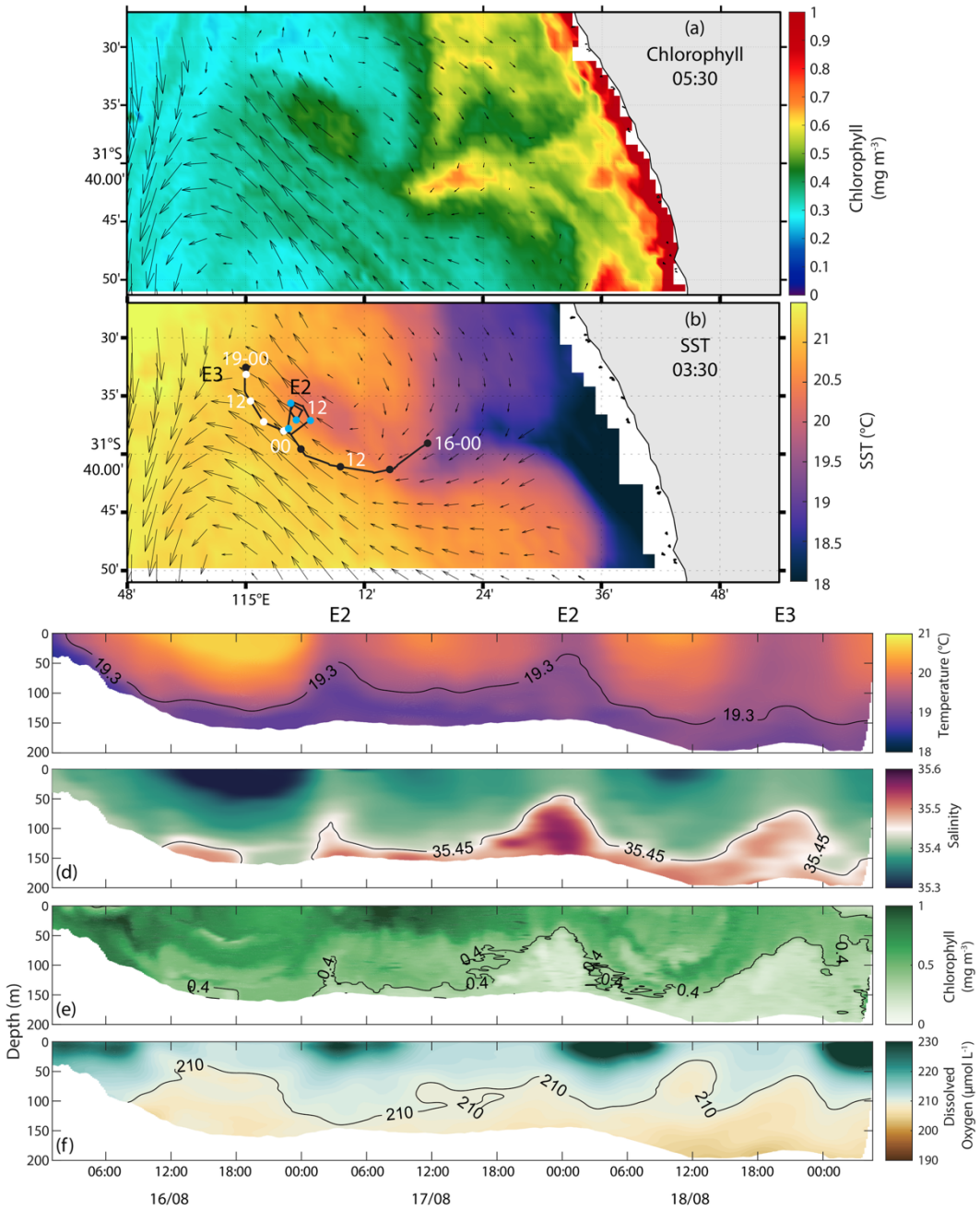

Figure 5. (a) SCC, (b) Sea Surface Temperature and HFR surface currents (vectors) on 16 August 2010. The black line represents glider track between 16-19 August 2010 (eddies #2-3, Event #1). The dots are at 6-hour intervals and colour codes according to date: 16 (black), 17 (blue), 18 (white). Along-track glider distribution of (c) temperature, (d) salinity, (e) G-Chl, and (f) dissolved oxygen. E2 and E3 refer to eddy numbers show in Table 2.

3.2 Event 2 (ocean moorings): Sub-mesoscale eddy dynamics – (April 2010)

Several cyclonic and anti-cyclonic eddies and peddies were observed within the HFR coverage and in proximity of the mooring sites between 16-21 April 2010 (Fig. 6). These features occurred under low to moderate (5-10 m s^{-1}) southerly and southeasterly wind conditions (Table 2) and all showed signatures of upwelling/downwelling.

Isotherm displacements consistent with upwelling were observed in temperature profiles at WATR15 and WATR20 moorings when a sub-mesoscale cyclonic eddy (24 km radius; Table 2) was detected on HFR currents on April 16. This eddy feature caused a vertical displacement of ~80m in the isotherms across moorings (eddy #4, Figs. 6a, 7d-f).

A similar response was observed on 17 April when an anti-cyclonic peddie (8 km radius; Table 2) crossed WATR20 and WATR50 moorings, uplifting waters up to 100m towards the surface (eddy #5, Figs. 7d-i). At the inner shelf, WATR05 mooring showed displacement of warmer water (~21.97°C) induced by an anti-cyclonic feature (eddy #6, Figs. 6b,c; 7a).

In the offshore region, an anti-cyclonic sub-mesoscale eddy (15 km radius; Table 2) approached the offshore mooring site (WATR50) on 18 April which vertically displaced isotherms by ~80m and reversed currents in the deeper layers (eddy #7, Figs. 6d; 7g-h). Along the inner shelf, a cold core cyclonic peddie (~8 km radius) was observed near WATR15 which persisted until 19 April with variable dimensions (Table 2), transporting a patch of higher SCC at its periphery with a ~130 m vertical displacement of the 21°C isotherm (eddy #8, Figs. 6d-f, i,j; 7b,c). Inshore of the cyclonic peddie, an anti-cyclonic peddie also uplifted waters in the region (eddy #9, Figs. 6e, 7a,b). Offshore, a cold core anti-cyclonic eddy (eddy #10, 28 km radius) transported moderate-to-high SCC at its centre (Table 2; Figs. 6i,j).

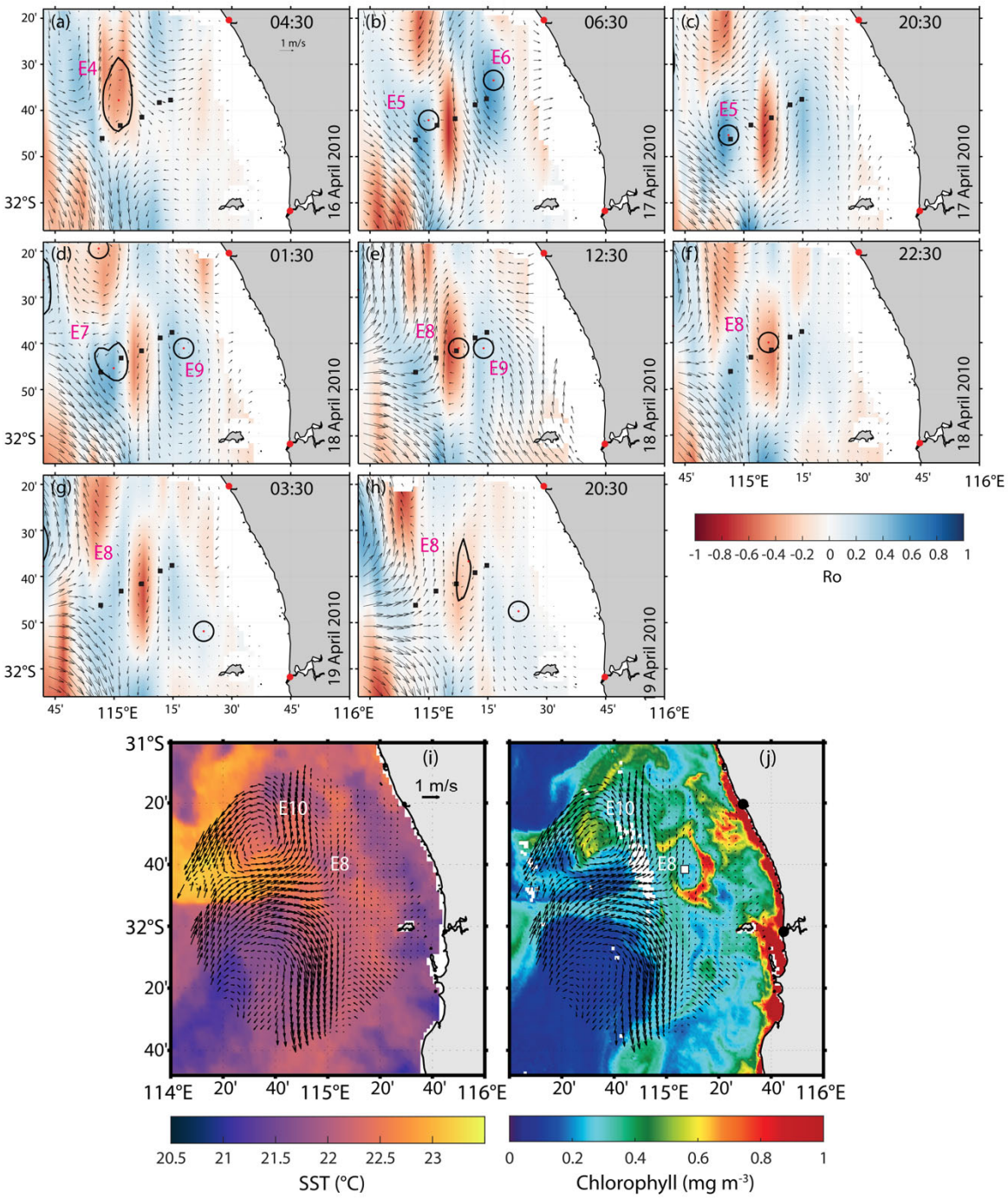

Figure 6. (a-h) HFR-derived Rossby number (in colour) and surface currents (vectors) occurring on 16-21 April 2010 (eddies #4-10, Event #2). (i) Sea Surface Temperature, (j) SCC, and HFR-derived surface currents (vectors) on 19 April 2010. In (a-h, j), mooring locations (Fig. 1c) are shown as black squares. Red dots and thicker black closed contour lines in (a-h) represent eddy centres and their shapes detected by the vector geometry algorithm. E4-E10 refer to eddy numbers shown in Table 2.

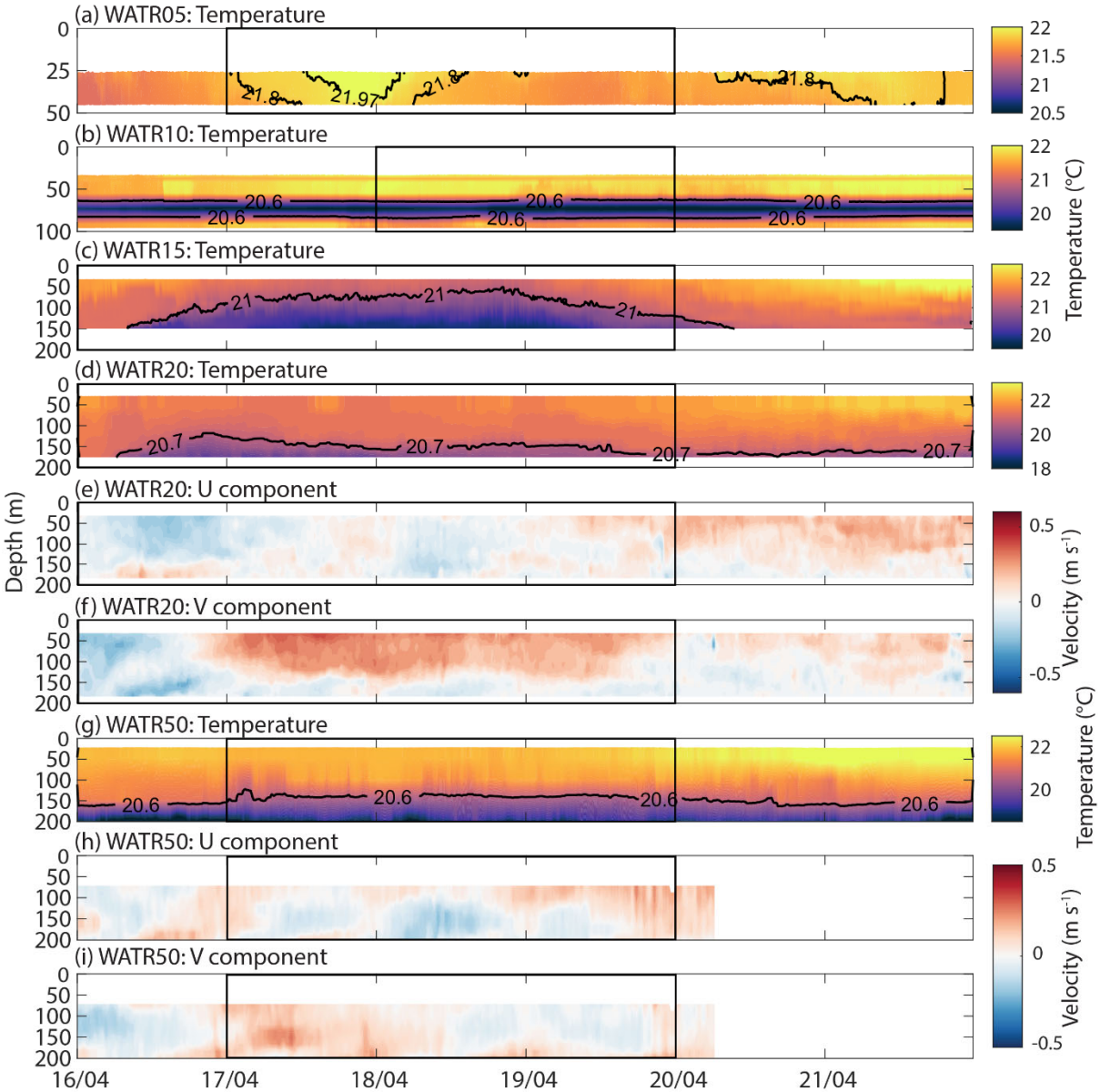

Figure 7. Mooring observations at (a) WATR05, (b) WATR10, (c) WATR15, (d-f) WATR20, and (g-i) WATR50 during 16 to 21 April 2010 (eddies #4-10, Event #2) for (a,b,c,d,g) temperature, (e,h) u component, and (f,i) v component. Black squares refer to eddy events shown in Fig. 6. Mooring locations are shown in Figs. 1c, 6.

3.3 Event 3 (ocean glider/mooring): Sub-mesoscale eddy and wind forcing – (February 2014)

On 16 February 2014, an anti-cyclonic peddie (eddy #11, 8 km radius) was present along the inner shelf and close to the moorings (Table 2; Figs. 8a-c) under strong (>10 m s^{-1}) southerly winds. Contrasting downwelling/upwelling signatures were identified at its centre and its periphery (Figs. 8d-f). An ocean glider tracked its southward movement and captured T, S, and G-Chl stratification with a subsurface DO maximum between ~40-60 m depth (Figs.

8g-j). Whilst the peddie feature dissipated around midnight, measurements showed an upwelling feature in both temperature and salinity structures (0.4 km in radius; Table 2) aligned with strong currents and a high Rossby number ($|R_o|$~15; Figs. 8c,g,h).

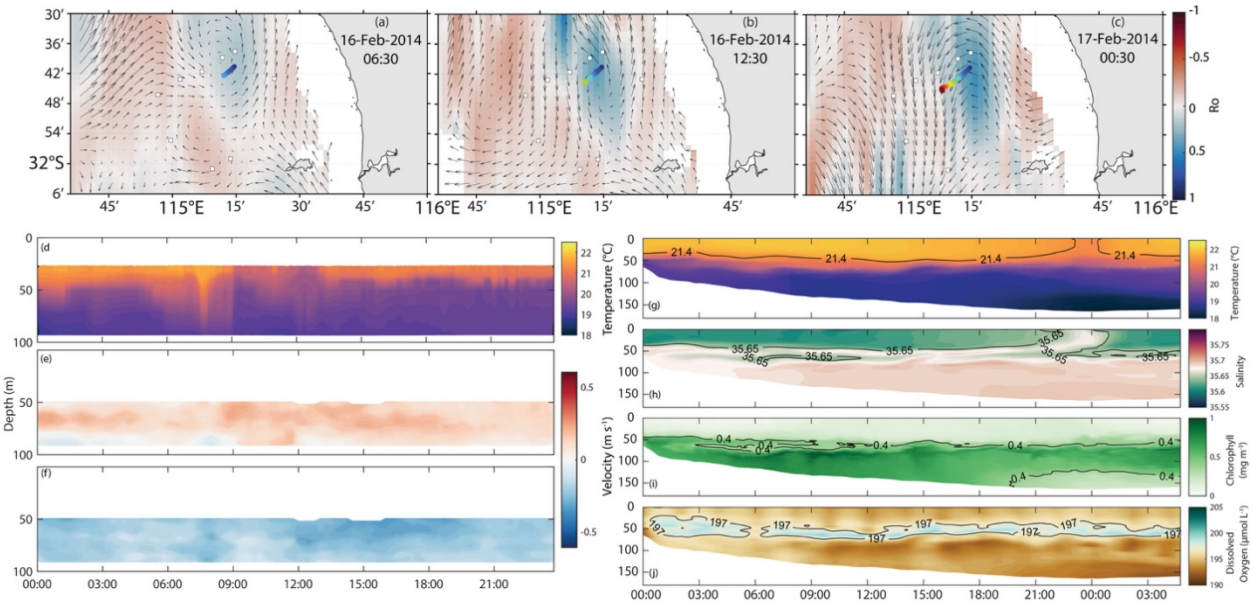

Figure 8. (a-c) HFR-derived Rossby number (in colour), surface currents (vectors), and glider tracking (in colour) on 16-17 February 2014 (eddy #11, Event #3). Mooring observations at WATR10 on 16 February 2014 for (d) temperature, (e) u component, and (f) v component. Cross-sectional ocean glider section on 16 February 2014 for (g) temperature, (h) salinity, (i) G-Chl, and (j) dissolved oxygen.

The dynamics at the periphery of an anti-cyclonic sub-mesoscale eddy and a small peddie under moderate (<10 m s^{-1}) southerly winds were captured later in February when the glider moved from the inner shelf towards deeper water (eddy #12, Table 2; Fig. 9a). Along the periphery of the sub-mesoscale eddy in the inner shelf, colder and salty waters contrasted with warmer and lower-salinity waters offshore associated with the Leeuwin Current. Inside the peddie, isotherms (and isohalines) were uplifted to reach the surface within a few hours from its appearance. Despite the low velocities, the peddie (1 km radius; Table 2; Fig. 9) had $|R_o|$~3.

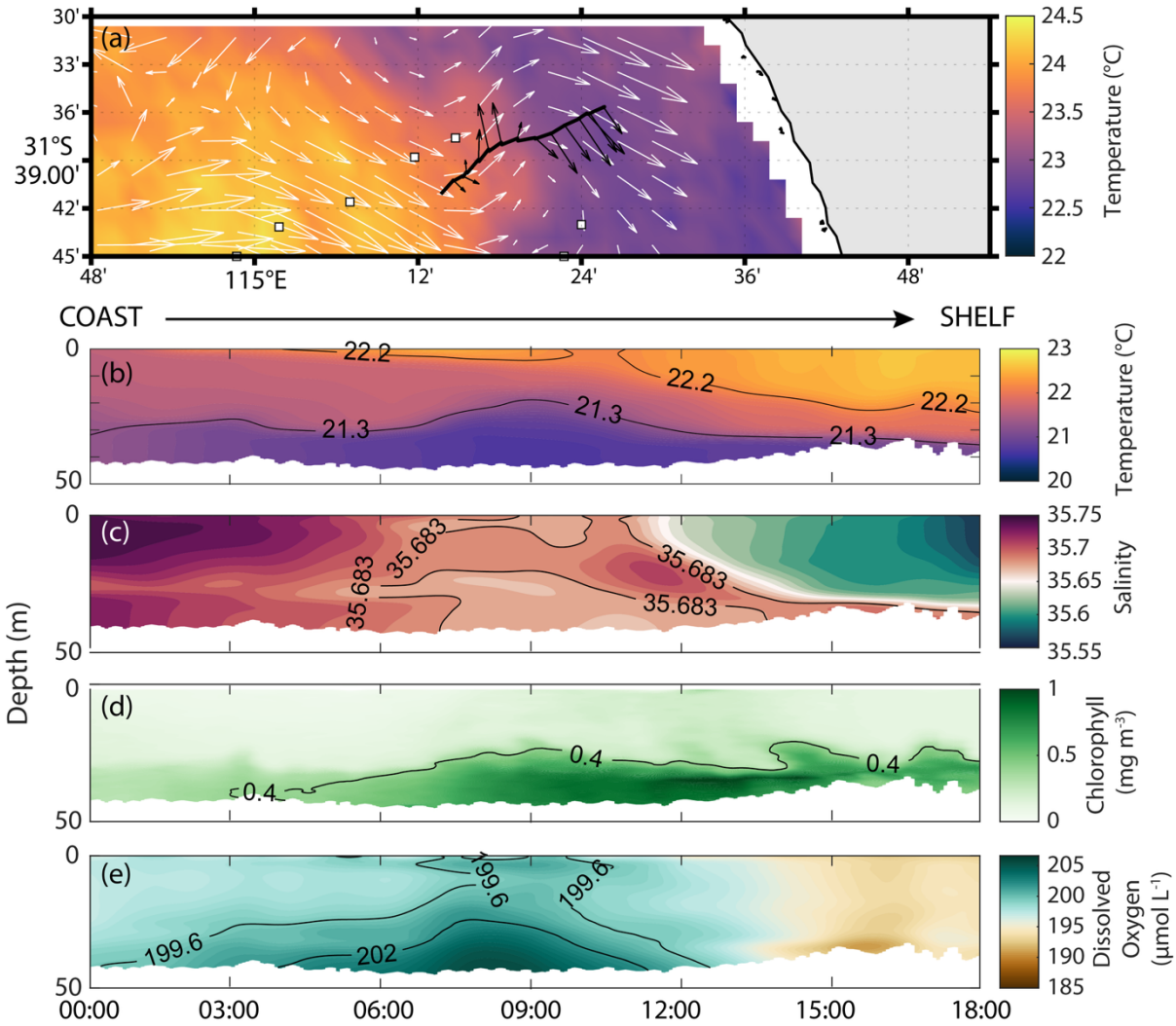

Figure 9. (a) Sea Surface Temperature and HFR surface currents (vectors) on 23 February 2014 (eddy #12, Event #3). Glider track and its depth-averaged velocities are shown in black in (a). Glider section along the tracking for (b) temperature, (c) salinity, (d) G-Chl, and (e) dissolved oxygen. Mooring locations are shown in (a) as black-white squares (see also Fig. 1c).

3.4 Event 4: Peddies Alley (ocean glider): fountains in the ocean (May – June 2015)

A glider deployment under different wind conditions was undertaken between 26 May and 02 June 2015. The winds were variable with (1) weak (~3 m s^{-1}) southeasterly winds 26-27 May; (2) easterly and southerly winds 28-30 May; and (3) strong (>10 m s^{-1}) northerly and north-westerly winds 01-02 June (Table 2). During 26-27 May 2015, the ocean glider travelled along the periphery of a cyclonic sub-mesoscale eddy and documented colder, saltier, denser waters to be uplifted within a peddie (eddy #13, 1 km radius; Table 2). The event occurred ~21:00 on 26 May (Fig. 10). Even under weak currents (<0.3 m s^{-1}; Fig. 10h-i) and strong Rossby number ($|R_o|$>5), higher G-Chl and oxygenated waters prevailed close to the seabed (Fig. 10).

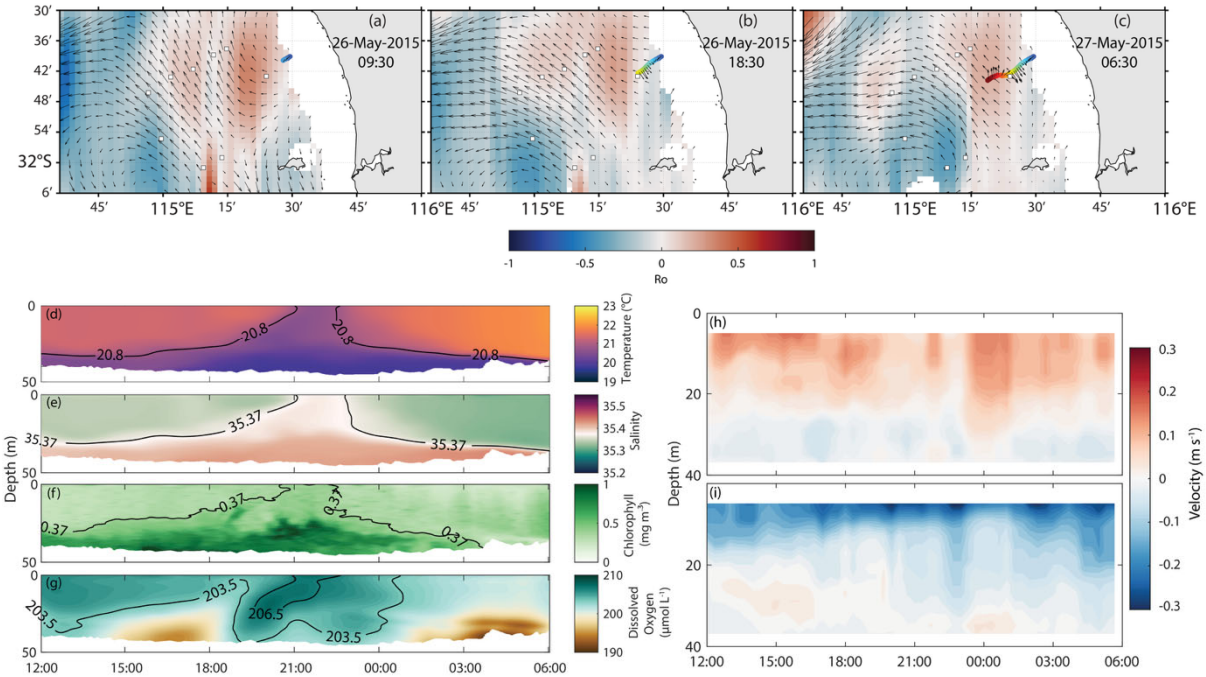

Figure 10. (a-c) HFR-derived Rossby number (in colour), surface currents (vectors), and glider tracking (in colour) on 26-27 May 2015 (eddy #13, Event #4). Cross-sectional ocean glider section on 26-27 May 2015 for (d) temperature, (e) salinity, (f) G-Chl, and (g) dissolved oxygen. Mooring locations are shown in (a-c) as black-white squares. Mooring observations at WATR04 (Fig. 1c) during 26-27 May 2015 for (h) u component, and (i) v component.

On 28-30 May 2015, the ocean glider mission continued tracking a region within high-G-Chl water entrainment (Fig. 11a). Closer to the shelf break, a peddie (eddy #14, 5 km radius; Table 2) displaced colder, more saline, denser waters with strong currents and Rossby number ($|R_o|$~8) restraining higher G-Chl and DO close to the surface (Peddie #1; Fig. 11). On the inner shelf, a patch of colder and dense water was trapped within a small peddie (eddy #15, 1 km radius; Table 2) in a region under higher G-Chl and lower DO (Peddie #2; Figs. 11a-d).

Although the peddie's currents were weaker on the inner shelf, Rossby number $|R_o|>5$ was recorded.

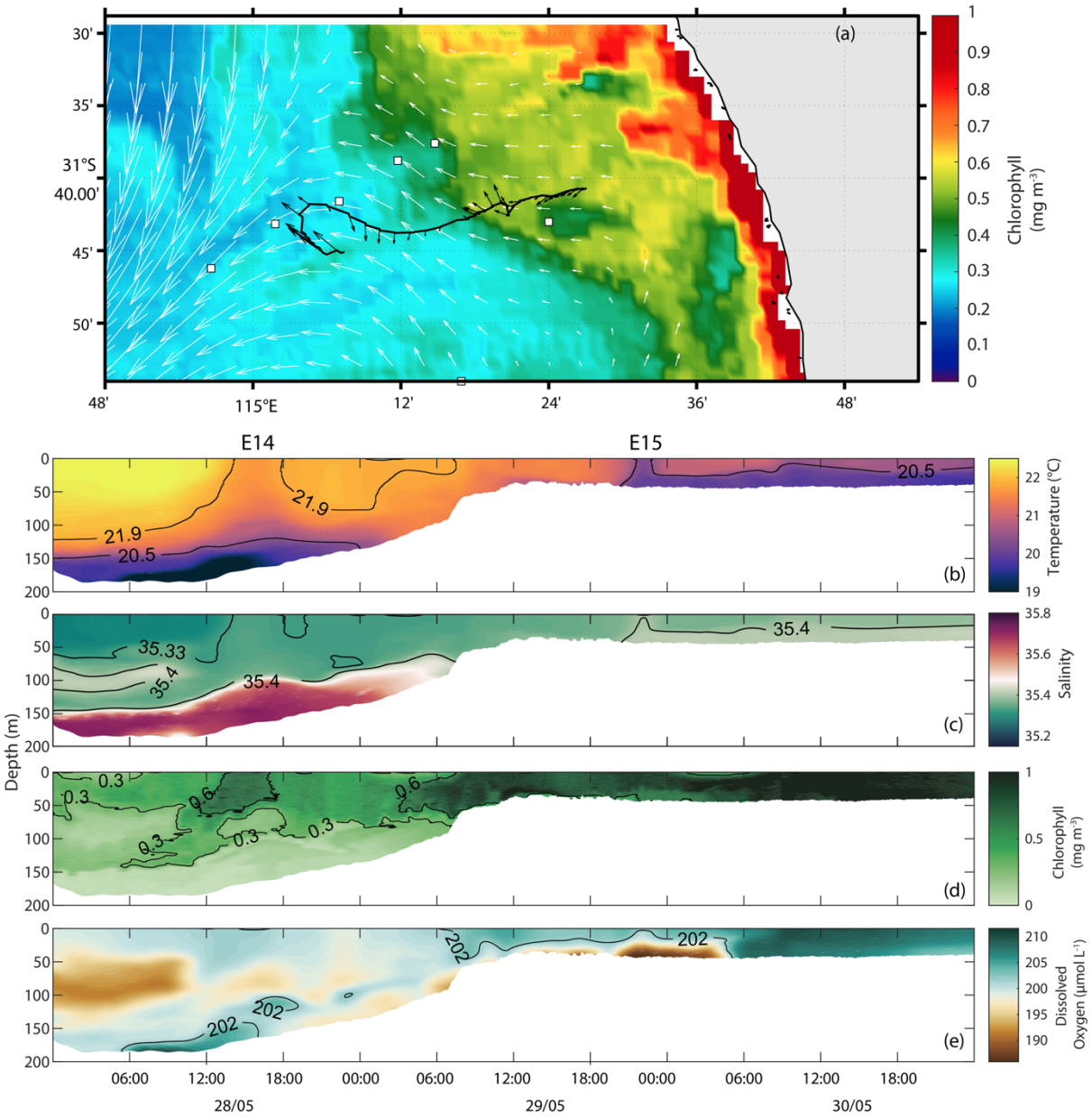

Figure 11. (a) SCC and HFR surface currents (vectors) on 30 May 2015 (Event #4). The black line represent glider track from 28 to 30 May 2015 (eddies #14-15, Event #4). Glider section along the tracking for (b) temperature, (c) salinity, (d) chlorophyll-a fluorescence, and (e) dissolved oxygen. Mooring locations are shown in (a) as black-white squares (see also Fig. 1c). E14 and E15 refer to eddy numbers shown in Table 2.

Several peddies were identified close to the coast and towards the inner shelf during 01-02 June 2015 (Table 2; Fig. 12). Near the coast, colder (18-19.6°C), denser, and saltier (35.44) waters were partially trapped in a peddie (eddy #16, 2 km radius) with weak currents (~0.3 m s^{-1}) and high Rossby number ($R_o>10$). This feature uplifted G-Chl (~1 mg m^{-3}) and

highly oxygenated (>208 μmol L^{-1}) waters towards the surface (Fig. 12). Another peddie (eddy #17, 2 km radius) with weak currents and a high Rossby number ($|R_o|$~10) was depicted around ~15-18h with warmer (20.1°C) and slightly lower salinity (35.40) waters. This feature transported G-Chl (~1 mg m^{-3}) and low-to-moderate DO concentrations (~203.5-206 μmol L^{-1}) towards the surface (Fig. 12). The last peddie (eddy #18, 1 km radius) was observed on 2 June around midnight with stronger currents (~0.5 m s^{-1}) and Rossby number ($|R_o|$>10), warmer (20.3°C) and lower-salinity (35.4) core with moderate G-Chl (~0.5 mg m^{-3}) and low DO (203 μmol L^{-1}) along the entire peddie structure (Fig. 12).

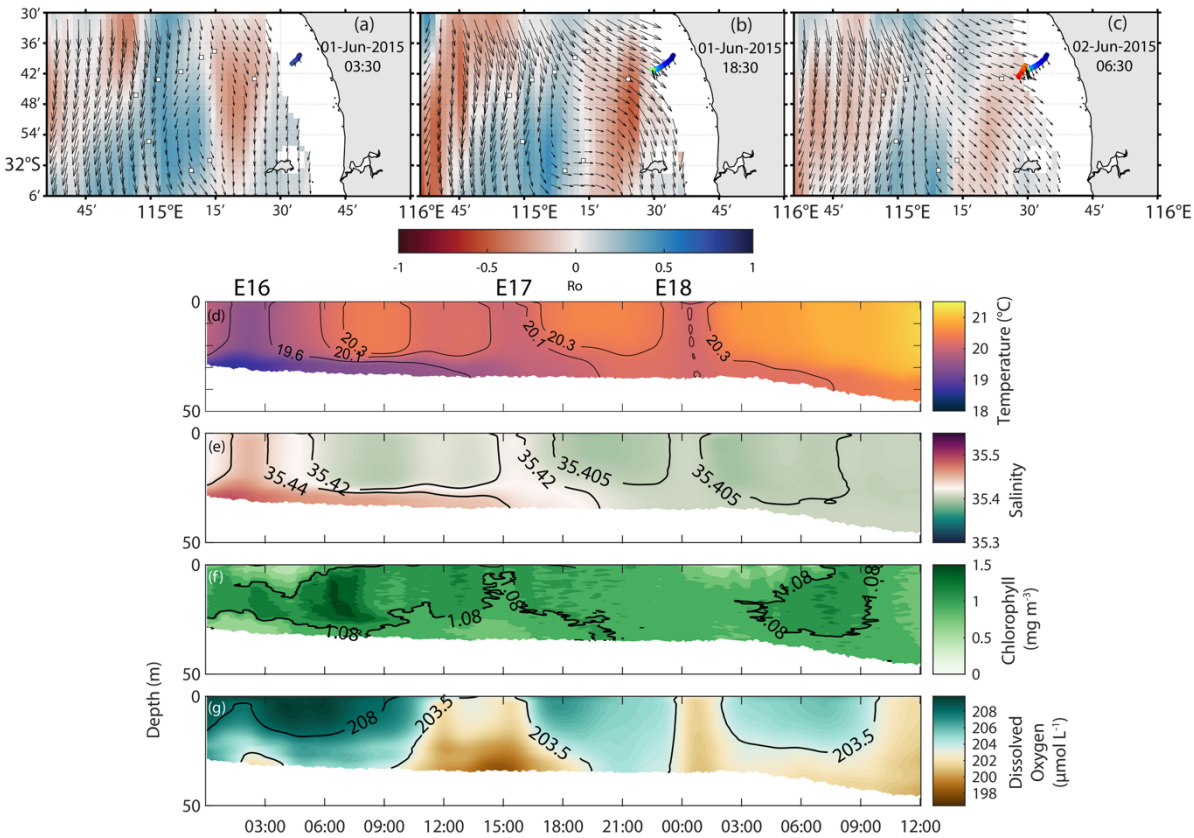

Figure 12. (a-c) HFR-derived Rossby number (in colour), surface currents (vectors), and glider tracking (in colour) on 01-02 June 2015 (eddies #16-18, Event #4). Cross-sectional ocean glider section on 01-02 June 2015 for (d) temperature, (e) salinity, (f) G-Chl, and (g) dissolved oxygen. Mooring locations are shown in (a-c) as black-white squares (see also Fig. 1c). E16-E18 refer to eddy numbers shown in Table 2.

4 Discussion

The simultaneous use of HFR, ocean gliders, moorings, satellite remote sensing, and shipborne measurements provides a rare multi-platform view of sub-mesoscale dynamics and their biogeochemical signature. By overcoming the spatial and temporal limitations of individual datasets, this approach offers insights into the three-dimensional physical and biogeochemical structure of sub-mesoscale eddies and their relationship with the forcing. It also allows us to link the observed eddies with the redistribution of dissolved oxygen and chlorophyll anomalies and to suggest a mechanism linking sub-mesoscale eddy upwelling to the uplift and redistribution of dense shelf water outflows. Overall, this multi-platform framework provides a comprehensive view of sub-mesoscale eddies, their circulation patterns and associated physical and biogeochemical structures, while providing direct evidence of their influence on biogeochemical variability in the Wadjemup Continental Shelf.

4.1 Sub-mesoscale eddy dynamics and their role in chlorophyll distribution

Along the Wadjemup Continental Shelf (WCS), sub-mesoscale eddies are short-lived (<12 h) but ubiquitous features, particularly in regions with high horizontal shear along the interfaces of the Leeuwin Current and the periphery of mesoscale eddies (Figs. 2, 5; Bitencourt et al., 2025). Our observations, however, indicate that they can last for longer periods (up to three days) and may exert a more sustained influence on the shelf circulation and biogeochemistry (Figs. 2-4).

Most eddies exhibited high Rossby numbers ($|R_o|>1$, Table 2), indicative of ageostrophic dynamics, and intense vertical transport (Table 2), which modulated biogeochemical distribution along the shelf (e.g., Figs. 2-5). In particular, cyclonic eddies had $|R_o|>1$ and upwelled chlorophyll-rich, highly oxygenated waters from depths greater than 25 m (Table 2; Figs. 3-5,10-12). These vertical velocities are consistent with previous theoretical and observational studies showing that sub-mesoscale eddies can generate intense vertical motions capable of transporting nutrients into the euphotic zone (e.g., Lévy et al., 2012; McWilliams, 2016). High Rossby numbers associated with submesoscale features indicate that processes other than geostrophic balance become important. In these conditions, centrifugal acceleration may play a significant role, potentially leading to gradient-wind or cyclostrophic balance, especially within compact and intense vortices (e.g., McWilliams, 2016; Thomas et al., 2008).

Cyclonic sub-mesoscale eddies and peddies with $|R_o|>5$ were particularly associated with strong upwelling (up to 185 m, Table 2) and cyclostrophic balance (Figs. 5, 10–12),

indicating intense vertical exchange within these structures. Anti-cyclonic eddies generally exhibited lower Rossby numbers ($|R_o|<1$) and were associated with downwelling of shallow waters (~50 m; Table 2). However, anti-cyclonic eddies observed during event #2 (16–21 April 2010) were also associated with upwelling (Figs. 6c, d; 7b–d) and cyclostrophic balance despite their relatively low Rossby numbers ($|R_o|<1$; Table 2). This apparent discrepancy may reflect an underestimation of vorticity due to the relatively coarse spatial resolution of the HFR measurements, which would smooth velocity gradients and reduce the calculated Rossby numbers.

Sub-mesoscale eddies (and peddies) redistributed chlorophyll along the shelf through both horizontal advection and local accumulation (Figs. 2a-c, 5, 6i,j). Cyclonic eddies tended to accumulate chlorophyll along their periphery, whereas anti-cyclonic eddies retained it closer to their centres (Figs. 6i, j), consistent with observations in other coastal systems (Davila et al., 2021; Veatch et al., 2024). High DO concentrations within these eddies (e.g., Fig. 5) are consistent with enhanced photosynthetic production relative to local biological consumption. By rapidly injecting nutrients into the euphotic zone (e.g., Bassin et al., 2005), these features may stimulate phytoplankton growth, trigger short-term blooms, and alter local primary production, with cascading effects on the structure and functioning of marine food webs (Figs. 2–5; Lévy et al., 2001, 2012). Mushroom-like structures were frequently associated with elongated chlorophyll filaments extending offshore (Fig. 1a), indicating strong lateral advection between adjacent eddies and enhanced transport of phytoplankton biomass. In oligotrophic regions such as the WCS, these processes can represent an important source of nutrients to coastal waters and create favourable feeding environments for larval species (Bitencourt et al., 2025).

4.2 Wind influence and dense water transport on sub-mesoscale eddies

Winds in the Wadjemup Continental Shelf control the circulation processes along the shelf in the absence of strong tidal forcing (Bitencourt et al., 2024; Mihanović et al., 2016). Previous work showed that southerly or southeasterly winds of ~7–8 m s^{-1} enhance pre-existing shear zones and promote the formation of sub-mesoscale eddies, whilst stronger winds (>11–12 m s^{-1}) tend to disrupt or dissipate these structures (Bitencourt et al., 2025).

Under sea breezes and southerly winds on February 23, 2014, for example, eddy structures emerged to the surface (Table 2; Fig. 9). Diurnal sea-breeze cycle in WCS can efficiently generate near-inertial waves due to the local inertial period (~24 h) that closely

matches the diurnal wind forcing (Mihanović et al., 2016). These waves can propagate energy downward and enhance vertical shear well below the mixed layer (Mihanović et al., 2016), potentially contributing to the vertical mixing and thermohaline anomalies observed during periods of strong wind forcing (Fig. 9).

Our observations during 16 February 2014 exhibit the influence of strong southerly winds (>11 m s^{-1}) on evolution and stability (Fig. 8). As winds intensified, the eddy structure became increasingly elongated and eventually destabilized (Figs. 8a–c). This evolution coincided with colder and more saline waters reaching the surface (Figs. 8g, h), consistent with enhanced vertical mixing and upwelling. Strong winds may also contribute to eddy decay by extracting energy through wind stress curl (Teng et al., 2023) and by enhancing surface turbulence and vertical mixing (Zhang and Tian, 2014; Zhu et al., 2023).

In the WCS, Dense Water Shelf Transport (DWST) is a common occurrence due to strong air-sea heat fluxes associated with the Mediterranean climate, which generate dense waters that propagate offshore as gravity currents along the seabed (Mahjabin et al., 2019a; Pattiaratchi et al., 2011). Previous studies showed that dense shelf water transport/cascading off Western Australia is predominantly seasonal, occurring mainly during austral autumn and winter when evaporation-driven salinity increases and surface cooling enhance nearshore water density gradients (Mahjabin et al., 2019, 2020). Our observations indicate that sub-mesoscale eddies (including peddies) can interact with these dense shelf water outflows (Figs. 5, 10-12). In particular, cyclonic sub-mesoscale eddies with $|R_o|>1$ entrained and uplifted portions of these dense shelf waters into the upper water column, with stronger DSWT uplift occurring under southerly winds and weaker uplift under northerly winds (Table 2; Figs. 5a, b; 10–12).

These observations suggest that sub-mesoscale eddies can play an active role in modulating the vertical transport and redistribution of dense shelf water outflows within the WCS (e.g., Fig. 5). In particular, these eddies may enhance vertical pumping of dense shelf waters and contribute to their redistribution within the upper water column (Table 2). Similar interactions between sub-mesoscale eddies and dense shelf water outflows have been reported in other coastal regions (Bosse et al., 2016; Fayman et al., 2019; Georgiou et al., 2020), highlighting the role of sub-mesoscale dynamics in modulating both horizontal and vertical transport along continental shelves.

4.3. Rossby number sensitivity and Force balance

Our multi-platform data set exhibited a wide range of Rossby numbers (R_o) across the selected events (Table 2). However, the different methods used to estimate R_o (Section 2.7) may introduce methodological uncertainties that affect direct comparisons between platforms. To ensure consistency, we recomputed R_o using a common formulation, $R_o = \frac{V}{fR}$, where V is the characteristic velocity, f is the Coriolis parameter and R the radius of curvature.

Using this formulation, R_o shows considerable differences between platforms (Fig. 13a) and previously calculated R_o (Table 2). For instance, the ship-based R_o during Event 1 indicates $|R_o|$~1, suggesting a flow regime where inertial and Coriolis forces are comparable. The HFR-derived R_o matching with ship-based observations (HFR-ship) on 3 August 2010 (Figs. 2,3; Event 1, Table 2) shows a smaller value, indicating stronger rotational control and a greater influence of Coriolis forces. In contrast, ocean glider-derived R_o (Events 1, 3 and 4; Table 2) span a much wider range ($|R_o|$~1–20), with many observations exceeding 1. This indicates strongly ageostrophic conditions and suggests that centrifugal effects may become significant (Fig. 13a). HFR-derived R_o remain consistently small ($|R_o|$<0.5), implying that the flow appears predominantly geostrophic and/or that smaller features (≤10 km diameter) may be underestimated due to HFR relatively coarse spatial resolution.

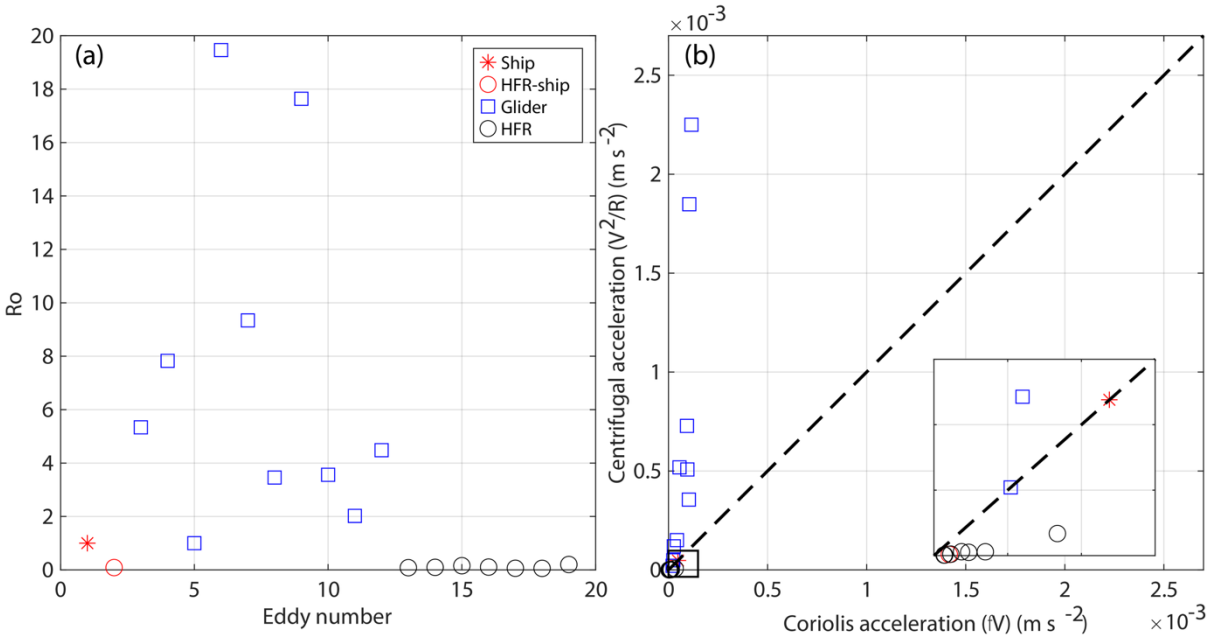

Figure 13. (a) Rossby number (R_o=V/(fR)) estimated for the selected events using different observing platforms: ship (red asterisk), HFR–ship (red circle) matching with ship transect (Event 1), glider (blue square), and HFR (black circle). (b) Centrifugal acceleration (V^2/R) versus Coriolis acceleration (fV). The dashed line in (b) indicates the 1:1 relationship (cyclogeostrophic balance).

We also compared centrifugal and Coriolis accelerations to further evaluate their relative influence in these features. Most HFR observations cluster near zero, indicating weak centrifugal contributions relative to Coriolis acceleration and a predominantly geostrophic regime (Fig. 13b). The ship and HFR-ship estimates lie close to the 1:1 line ($V^2/R \approx fV$) (Fig. 13b), consistent with cyclogeostrophic balance, where centrifugal and Coriolis forces are of comparable magnitude ($|R_o| \sim 1$). This suggests that HFR measurements mainly reflect larger-scale flows that remain closer to geostrophic balance.

Several ocean glider observations, in contrast, exhibited centrifugal accelerations comparable to or exceeding Coriolis acceleration (Fig. 13b), consistent with the large Rossby numbers inferred from ocean glider data (Table 2, Fig. 13a) and suggests a transition toward cyclostrophic balance, where centrifugal effects become dominant. Overall, this suggests that ocean glider measurements capture smaller-scale, more nonlinear structures where centrifugal effects become important.

5 Conclusions

This study investigated the physical and biogeochemical three-dimensional structure of sub-mesoscale eddies and peddies along the Wadjemup (Rottnest) Continental Shelf (Western Australia). A multi-platform data set was used, consisting of remote sensing, shipborne, mooring, and ocean glider measurements. Analyses outlined the role of a mesoscale eddies in the generation of sub-mesoscale eddies, their internal structures under different forcing conditions, and their potential contribution to chlorophyll distribution. The main conclusions can be summarised as follows:

- Sub-mesoscale eddies were found to occur primarily in areas of high shear, such as at the edges of Leeuwin Current, where the LC interacted with the wind-driven Capes Current, and at the periphery of larger mesoscale features in agreement with Bitencourt et al. (2025). Local winds contributed to the generation and dissipation of surface and near-surface eddies, also leading to the surfacing of underwater eddies.
- Localised upwelling and downwelling conditions commonly occurred within the eddies. Upwelling of isotherms (up to 185 m vertically) was recorded within cyclonic sub-mesoscale eddies. Anti-cyclonic eddies were found to promote both downwelling and upwelling.
- Mesoscale and sub-mesoscale eddies could lead to elevated chlorophyll levels in offshore regions and concentrations of high chlorophyll due to advection throughout

the study area. In the presence of dense water outflows, sub-mesoscale eddies trapped, upwelled, and transported some of these waters offshore.

Data Availability

All the data used in this study are publicly available. Data are available from https://portal.aodn.org.au/, as part of the Australian Integrated Marine Observing System (IMOS), which is enabled by the National Collaborative Research Infrastructure Strategy (NCRIS). All figures were generated using MATLAB software from MathWorks, Inc (http://www.mathworks.com), R2022b.

Author Contributions

This study was done as a part of PhD research by LPB. All data analysis were done by LPB with the supervision of CBP, SC, and YH. All authors have read and agreed to the published version of the manuscript.

Competing interests

The authors declare that the research was conducted in the absence of any commercial or financial relationships that could be construed as a potential conflict of interest. One of the co-authors (CP) is an editor of the Ocean Science special issue 'Advances in ocean science from underwater gliders'.

Acknowledgments

The Ocean Glider, Moorings, High Frequency Radar (HFR) surface currents and satellite Sea Surface Temperature data used in this study were sourced from Australia's Integrated Marine Observing System (IMOS). IMOS is enabled by the National Collaborative Research Infrastructure Strategy (NCRIS). It is operated by a consortium of institutions as an unincorporated joint venture, with the University of Tasmania as Lead Agent. We are also thankful to Australian Bureau of Meteorology (BOM) for making wind data available, and the Commonwealth Scientific and Industrial Research Organisation (CSIRO) for the ship measurements. LPB received the International Research Fees (SIRF) and University Postgraduate Award (UPA) Scholarships.

References

Akpınar, A., Charria, G., Theetten, S., & Vandermeirsch, F. (2020). Cross-shelf exchanges in the northern Bay of Biscay. Journal of Marine Systems, 205, 103314.

Akpınar, A., Sadighrad, E., Fach, B. A., & Arkın, S. (2022). Eddy induced cross-shelf exchanges in the Black Sea. Remote Sensing, 14(19), 4881.

Aleskerova, A., Kubryakov, A., Stanichny, S., Medvedeva, A., Plotnikov, E., Mizyuk, A., & Verzhevskaia, L. (2021). Characteristics of topographic submesoscale eddies off the Crimea coast from high-resolution satellite optical measurements. Ocean Dynamics, 71(6), 655-677.

Bitencourt, L. P., Pattiaratchi, C. B., Cosoli, S., & Hetzel, Y. (2024). Long-term surface current variability across the continental shelf and slope. Journal of Geophysical Research: Oceans, 129(9), e2023JC020214.

Bitencourt, L. P., Pattiaratchi, C., Cosoli, S., and Hetzel, Y. (2025). Shear-induced sub-mesoscale eddies along an eastern boundary current. Journal of Physical Oceanography. 55(12), 2491–2541, doi: 10.1175/JPO-D-24-0129.1.

Bosse, A., Testor, P., Houpert, L., Damien, P., Prieur, L., Hayes, D., ... & Mortier, L. (2016). Scales and dynamics of Submesoscale Coherent Vortices formed by deep convection in the northwestern Mediterranean Sea. Journal of Geophysical Research: Oceans, 121(10), 7716-7742.

Bosse, A., Testor, P., Mayot, N., Prieur, L., d'Ortenzio, F., Mortier, L., Le Goff, H., Gourcuff, C., Coppola, L., Lavigne. H., & Raimbault, P. (2017). A submesoscale coherent vortex in the Ligurian Sea: From dynamical barriers to biological implications. Journal of Geophysical Research: Oceans, 122(8), 6196-6217.

Bouffard, J., Renault, L., Ruiz, S., Pascual, A., Dufau, C., & Tintoré, J. (2012). Sub-surface small-scale eddy dynamics from multi-sensor observations and modeling. Progress in Oceanography, 106, 62-79.

Bourg, N., Schaeffer, A., and Molcard, A. (2024). East Australian Current system: Frontal barrier and fine-scale control of chlorophyll-a distribution. Journal of Geophysical Research: Oceans, 129(3), e2023JC020312.

Brannigan, L. (2016). Intense submesoscale upwelling in anticyclonic eddies. Geophysical Research Letters, 43(7), 3360-3369.

Bui, T., & Feng, M. (2025). Gap-filled, gridded subsurface physical oceanography time series dataset derived from selected mooring measurements off the Western Australia coast during 2009–2023. https://doi.org/10.25919/myac-yx60

Capet, X., Campos, E. J., & Paiva, A. M. (2008). Submesoscale activity over the Argentinian shelf. Geophysical Research Letters, 35(15).

Chelton, D. B., Schlax, M. G., Samelson, R. M., & de Szoeke, R. A. (2007). Global observations of large oceanic eddies. Geophysical Research Letters, 34(15).

Chen, M., Pattiaratchi, C.B., Ghadouani, A. & Hanson, C. (2019). Seasonal and interannual variability of water column properties along the Rottnest continental shelf, south-west Australia. Ocean Science, 15, 333–348

Chen, J., Zhu, X. H., Zheng, H., & Wang, M. (2023). Submesoscale dynamics accompanying the Kuroshio in the East China Sea. Frontiers in Marine Science, 9, 1124457.

Cosoli, S., and Grcic, B. (2024). Quality Control procedures for IMOS Ocean Radar Manual, Version 3.0. Hobart, Australia, Integrated Marine Observing System, 98pp. DOI: http://dx.doi.org/10.26198/5c89b59a931cb

Cosoli, S., Pattiaratchi, C., & Hetzel, Y. (2020). High-frequency radar observations of surface circulation features along the south-western Australian coast. Journal of Marine Science and Engineering, 8(2), 97.

Cresswell, G. (1996). The Leeuwin Current near Rottnest Island, Western Australia. Marine and Freshwater Research, 47(3), 483-487.

Damien, P., Bianchi, D., Kessouri, F., & McWilliams, J. C. (2023). Modulation of phytoplankton uptake by mesoscale and submesoscale eddies in the California current system. Geophysical Research Letters, 50(16), e2023GL104853. https://doi.org/10.1029/2023GL104853

Davila, X., Rubio, A., Artigas, L. F., Puillat, I., Manso-Narvarte, I., Lazure, P., & Caballero, A. (2021). Coastal submesoscale processes and their effect on phytoplankton distribution in the southeastern Bay of Biscay. Ocean Science, 17(3), 849-870.

Earp A, Hanson CE, Ralph PJ, Brando VE, Allen S, Baird M, Clementson L, Daniel P, Dekker AG, Fearns P, Parslow JS, Strutton PG, Thompson PA, Underwood M, Weeks S, and Doblin MA. 2011. Review of fluorescent standards for calibration of in situ fluorometers: Recommendations applied in coastal and ocean observing programs. Optics Express, 19, 26768-2678.

Fayman, P., Ostrovskii, A., Lobanov, V., Park, J. H., Park, Y. G., & Sergeev, A. (2019). Submesoscale eddies in Peter the Great Bay of the Japan/East Sea in winter. Ocean Dynamics, 69, 443-462.

Feng, M., Waite, A. M., & Thompson, P. A. (2009). Climate variability and ocean production in the Leeuwin Current system off the west coast of Western Australia. Journal of the Royal Society of Western Australia, 92, 67.

Feng, M., Bui, T., & Benthuysen, J. A. (2025). Seasonal climatology of the Leeuwin Current-Capes Current system off southwest Australia from long-term moored observations. Journal of Geophysical Research: Oceans, 130, e2025JC022662. https://doi.org/10.1029/2025JC022662

Ferrari, R., & Wunsch, C. (2009). Ocean circulation kinetic energy: Reservoirs, sources, and sinks. Annual Review of Fluid Mechanics, 41(1), 253-282.

Fieux, M., Molcard, R., & Morrow, R. (2005). Water properties and transport of the Leeuwin Current and eddies off Western Australia. Deep Sea Research Part I: Oceanographic Research Papers, 52(9), 1617-1635.

Fu, L. L., Alsdorf, D., Rodriguez, E., Morrow, R., Mognard, N., Lambin, J., ... & Lafon, T. (2009). The SWOT (Surface Water and Ocean Topography) mission: Spaceborne radar interferometry for oceanographic and hydrological applications. Proceedings of OCEANOBS, 9, 21-25.

Georgiou, S., Ypma, S. L., Brüggemann, N., Sayol, J. M., Pietrzak, J. D., & Katsman, C. A. (2020). Pathways of the water masses exiting the Labrador Sea: The importance of boundary–interior exchanges. Ocean Modelling, 150, 101623.

Gersbach, G. H., Pattiaratchi, C. B., Ivey, G. N., & Cresswell, G. R. (1999). Upwelling on the south-west coast of Australia—source of the Capes Current?. Continental Shelf Research, 19(3), 363-400.

Govekar, P. D., Griffin, C., & Beggs, H. (2022). Multi-sensor sea surface temperature products from the Australian Bureau of Meteorology. Remote Sensing, 14(15), 3785.

Guerrero, L., Sheinbaum, J., Mariño-Tapia, I., González-Rejón, J. J., & Pérez-Brunius, P. (2020). Influence of mesoscale eddies on cross-shelf exchange in the western Gulf of Mexico. Continental Shelf Research, 209, 104243.

Hanson, C. E., Woo, L. M., Thomson, P. G., & Pattiaratchi, C. B. (2017). Observing the ocean with gliders: techniques for data visualization and analysis. Oceanography, 30(2), 222-227.

He, Y., Feng, M., Xie, J., He, Q., Liu, J., Xu, J., et al. (2021). Revisit the vertical structure of the eddies and eddy-induced transport in the Leeuwin Current system. Journal of Geophysical Research: Oceans, 126. https://doi.org/10.1029/2020JC016556.

Irigoien, X., Fiksen, Cotano, U., Uriarte, A., Alvarez, P., Arrizabalaga, H., Boyra, G., Santos, M., Sagarminaga, Y., Otheguy, P., Etxebeste, E., Zarauz, L., Artetxe, I., and Motos, L. (2007). Could Biscay Bay Anchovy recruit through a spatial loophole?, Prog. Oceanogr., 74, 132–148, https://doi.org/10.1016/j.pocean.2007.04.011

Kendrick, G. A., Cambridge, M. L., Orth, R. J., Fraser, M. W., Hovey, R. K., Statton, J., ... & Sinclair, E. A. (2023). The cycle of seagrass life: From flowers to new meadows. Ecology and Evolution, 13(9), e10456.

Kodithuwakku, S., (2024). Dynamics of mesoscale eddies in the south-eastern Indian Ocean. Unpubl PhD Thesis, The University of Western Australia, https://doi.org/10.26182/5gqn-fk63

Kolodziejczyk, N., Testor, P., Lazar, A., Echevin, V., Krahmann, G., Chaigneau, A., Gourcuff, C., Wade, M., Faye, S., Estrade, P., Capet, X., Mortier, L., Brehmer, P., Schütte, F., & Karstensen, J. (2018). Subsurface fine-scale patterns in an anticyclonic eddy off cap-vert peninsula observed from glider measurements. Journal of Geophysical Research: Oceans, 123(9), 6312-6329.

Kubryakov, A. A., Puzina, O. S., and Mizyuk, A. I. (2022). Cross-Slope Buoyancy Fluxes Cause Intense Asymmetric Generation of Submesoscale Eddies on the Periphery of the Black Sea Mesoscale Anticyclones. Journal of Geophysical Research: Oceans, 127(6), e2021JC018189.

Lévy, M., Klein, P., & Treguier, A.-M. (2001). Impact of sub-mesoscale physics on production and subduction of phytoplankton in an oligotrophic regime. Journal of Marine Research, 59(4), 535–565. https://doi.org/10.1357/00222400176284218

Lévy, M., Iovino, D., Resplandy, L., Klein, P., Madec, G., Tréguier, A. M., Masson, S., and Takahashi, K. (2012). Large-scale impacts of submesoscale dynamics on phytoplankton: Local and remote effects. Ocean Modelling, 43, 77-93.

Lévy, M., Franks, P. J., & Smith, K. S. (2018). The role of submesoscale currents in structuring marine ecosystems. Nature communications, 9(1), 4758. 10.1038/s41467-018-07059-3

Lipinskaya, N. A., Salyuk, P. A., & Golik, I. A. (2023). Variations and Depth of Formation of Submesoscale Eddy Structures in Satellite Ocean Color Data in the Southwestern Region of the Peter the Great Bay. Remote Sensing, 15(23), 5600.

Liu, F., Tang, S., and Chen, C. (2015) Satellite observations of the small-scale cyclonic eddies in the western South China Sea. Biogeosciences, 12(2), 299-305.

Mahadevan, A. (2016). The impact of submesoscale physics on primary productivity of plankton. Annual review of marine science, 8(1), 161-184.

Mahadevan, A., and Tandon, A. (2006) An analysis of mechanisms for submesoscale vertical motion at ocean fronts. Ocean Modelling, 14(3-4), 241-256.

Mahjabin, T., Pattiaratchi, C., and Hetzel, Y. (2019a). Wind effects on dense shelf water cascades in south-west Australia. Continental Shelf Research, 189, 103975. https://doi.org/10.1016/j.csr.2019.103975

Mahjabin, T., Pattiaratchi, C., Hetzel, Y., and Janekovic, I. (2019b). Spatial and temporal variability of dense shelf water cascades along the Rottnest continental shelf in southwest Australia. Journal of Marine Science and Engineering, 7(2), 30. https://doi.org/10.3390/jmse7020030

McWilliams, J. C. (2016). Submesoscale currents in the ocean. Proceedings of the Royal Society of London. Series A, Mathematical and Physical Sciences, 472(2189), https://doi.org/10.1098/rspa.2016.0117

Mihanović, H., Pattiaratchi, C., and Verspecht, F. (2016). Diurnal sea breezes force near-inertial waves along Rottnest continental shelf, southwestern Australia. Journal of Physical Oceanography, 46(11), 3487-3508. https://doi.org/10.1175/JPO-D-16-0022.1

Morello, E. B., Galibert, G., Smith, D., Ridgway, K. R., Howell, B., Slawinski, D., et al. (2014). Quality Control (QC) procedures for Australia's National reference station's sensor data—Comparing semi-autonomous systems to an expert oceanographer. Methods in Oceanography, 9, 17–33. https://doi.org/10.1016/j.mio.2014.09.001

Morvan, M., L'hégaret, P., Carton, X., Gula, J., Vic, C., De Marez, C., Sokolovskiy, M., And Koshel, K. (2019) The life cycle of submesoscale eddies generated by topographic interactions, Ocean Sci., 15, 1531–1543, https://doi.org/10.5194/os-15-1531-2019.

Nencioli, F., Dong, C., Dickey, T., Washburn, L., & McWilliams, J. C. (2010). A vector geometry–based eddy detection algorithm and its application to a high-resolution numerical model product and high-frequency radar surface velocities in the Southern California Bight. Journal of atmospheric and oceanic technology, 27(3), 564-579.

Oguz, T., Macias, D., and Tintore, J. (2015) Ageostrophic frontal processes controlling phytoplankton production in the Catalano-Balearic Sea (Western Mediterranean). PLoS One, 10(6), e0129045.

O'Reilly, J.E. and Werdell, P.J.2019) Chlorophyll algorithms for ocean color sensors - OC4, OC5 & OC6. Remote Sensing of Environment, 229,32-47

Paduan, J. D., and Washburn, L. (2013). High-frequency radar observations of ocean surface currents. Annual review of marine science, 5, 115-136. https://doi.org/10.1146/annurev-marine-121211-172315

Parks, A. B., Shay, L. K., Johns, W. E., Martinez-Pedraja, J., and Gurgel, K. W. (2009). HF radar observations of small-scale surface current variability in the Straits of Florida. Journal of Geophysical Research: Oceans, 114(C8). https://doi.org/10.1029/2008JC005025

Pattiaratchi, C., James, A., & Collins, M. (1987). Island wakes and headland eddies: a comparison between remotely sensed data and laboratory experiments. Journal of Geophysical Research: Oceans, 92(C1), 783-794.

Pattiaratchi, C., & Buchan, S. J. (1991). Implications of long-term climate change for the Leeuwin Current. Journal of the Royal Society of Western Australia, 74, 133-140.

Pattiaratchi, C., and Eliot, M. (2009). Sea level variability in south-west Australia: from hours to decades. In Coastal Engineering 2008: pp. 1186-1198). http://dx.doi.org/10.1142/9789814277426_0099

Pattiaratchi C. and Hanson C., 2010: The RV Southern Surveyor. Voyage Plan ss2010_v06. https://www.marine.csiro.au/data/reporting/get_file.cfm?eov_pub_id=826

Pattiaratchi, C. and Mihanović, H. (2014). Peddies: what, where, why?. Proceedings of the Australian Coastal and Oceans Modelling and Observations Workshop (ACOMO). https://www.researchgate.net/publication/267631241_Peddies_what_where_why

Pattiaratchi, C., and Woo, M. (2009). The mean state of the Leeuwin current system between North West Cape and Cape Leeuwin. Journal of the Royal Society of Western Australia, 92, 221-241.

Pattiaratchi, C. B., and Siji, P. (2020). Variability in ocean currents around Australia. State and Trends of Australia's Ocean Report. Hobart. Integrated Marine Observing System (IMOS),1-6.

Pattiaratchi CB, Hollings B, Woo M & Welhena T. (2011) Dense shelf water formation along the south-west Australian inner shelf. Geophysical Research Letters, 38(10), L10609, doi: 10.1029/2011GL046816

Pattiaratchi, C., Woo, L. M., Thomson, P. G., Hong, K. K., and Stanley, D (2017) Ocean glider observations around Australia, Oceanography, 30(2), 90–91. https://doi.org/10.5670/oceanog.2017.226.

Pearce, A. F., and Griffiths, R. W. (1991). The mesoscale structure of the Leeuwin Current: a comparison of laboratory models and satellite imagery. Journal of Geophysical Research: Oceans, 96(C9), 16739-16757.

Pearce, A., and Pattiaratchi, C. (1999). The Capes current: a summer countercurrent flowing past Cape Leeuwin and Cape Naturaliste, Western Australia. Continental Shelf Research, 19(3), 401-420. https://doi.org/10.1029/91JC01712

Pond, S., & Pickard, G. L. (1983). Introductory dynamical oceanography. Gulf Professional Publishing.

Rafiq W.S. (2024). Sea Breeze Driven Diurnal Coastal Currents off the Southwest Australia, Unpubl. PhD Thesis. The University of Western Australia. 175pp

Rafiq, S., Pattiaratchi, C., and Janeković, I. (2020). Dynamics of the Land–Sea Breeze System and the Surface Current Response in South-West Australia. Journal of Marine Science and Engineering, 8(11), 931. https://doi.org/10.3390/jmse8110931.

Rennie, S. J., Pattiaratchi, C. P., and McCauley, R. D. (2007). Eddy formation through the interaction between the Leeuwin Current, Leeuwin Undercurrent and topography. Deep Sea Research Part II: Topical Studies in Oceanography, 54(8-10), 818-836. https://doi.org/10.1016/j.dsr2.2007.02.005

Richardson, L. E., Middleton, J. F., Kyser, T. K., James, N. P., & Opdyke, B. N. (2019). Shallow water masses and their connectivity along the southern Australian continental margin. Deep Sea Research Part I: Oceanographic Research Papers, 152, 103083.

Roarty, H., Cook, T., Hazard, L., George, D., Harlan, J., Cosoli, S, Wyatt, L, Fanjul, E, Terrill, E, Otero, M, Largier, J, Glenn, S, Ebuchi, N, Whitehouse, B, Bartlett, K, Mader, J, Rubio, A, Corgnati, L, Mantovani, C, Griffa, A, Reyes, E, Lorente, P, Flores-Vidal, X, Saavedra-Matta, KJ, Rogowski, P, Prukpitikul, S, Lee, S-H, Lai, J-W, Guerin, C-A, Sanchez, J, Hansen, B and Grilli, S. (2019). The global high frequency radar network. Frontiers in marine science, 6, 164. https://doi.org/10.3389/fmars.2019.00164

Rossi, V., Feng, M., Pattiaratchi, C., Roughan, M., & Waite, A. M. (2013). Linking synoptic forcing and local mesoscale processes with biological dynamics off Ningaloo Reef. Journal of Geophysical Research: Oceans, 118(3), 1211-1225.

Rubio, A., Caballero, A., Orfila, A., Hernández-Carrasco, I., Ferrer, L., González, M., Solabarrieta, L., and Mader, J. (2018). Eddy-induced cross-shelf export of high Chl-a coastal waters in the SE Bay of Biscay. Remote Sensing of Environment, 205, 290-304.

Rudnick, D. L., Gopalakrishnan, G., & Cornuelle, B. D. (2015). Cyclonic eddies in the Gulf of Mexico: Observations by underwater gliders and simulations by numerical model, J. Phys. Oceanogr., 45(1), 313-326, https://doi.org/10.1175/JPO-D-14-0138.1,6552015.

Rudnick, D. L. (2016). Ocean research enabled by underwater gliders. Annual review of marine science, 8(1), 519-541.

Ruiz, S., Pascual, A., Garau, B., Faugère, Y., Alvarez, A., & Tintoré, J. (2009). Mesoscale dynamics of the Balearic Front, integrating glider, ship and satellite data. Journal of Marine Systems, 78, S3-S16.

Schaeffer, A., A. Gramoulle, M. Roughan, and A. Mantovanelli (2017). Characterizing frontal eddies along the East Australian Current from HF radar observations, Journal of Geophysical Research: Oceans, 122, https://doi.org/10.1002/2016JC012171.

Siegel, D. A., Peterson, P., McGillicuddy Jr, D. J., Maritorena, S., & Nelson, N. B. (2011). Bio-optical footprints created by mesoscale eddies in the Sargasso Sea. Geophysical Research Letters, 38(13).

Taylor, J. R. (2016). Turbulent mixing, restratification, and phytoplankton growth at a submesoscale eddy. Geophysical Research Letters, 43(11), 5784-5792.

Teng, F., Dong, C., Lim Kam Sian, K. T. C., Ji, J., & Zhu, W. (2023). Wind work on oceanic mesoscale eddies in the Northeast Tropical Pacific Ocean. Frontiers in Marine Science, 10, 1202875.

Thomas, L. N., Tandon, A., and Mahadevan, A. (2008). Submesoscale processes and dynamics. Ocean modeling in an Eddying Regime, Geophys. Monogr., Vol. 177, Amer. Geophys. Union, 17–38, https://doi.org/10.1029/177GM04.

Thomson, P.G. Pattiaratchi, C.B. and Hanson, C.E. (2026) Understanding the stability of the ECOPuck optical sensor: evaluation 1 of long-term ocean glider data streams across decades. Frontiers in Marine Science, 13, https://doi.org/10.3389/fmars.2026.1703896

Trotter, J. A., Pattiaratchi, C., Montagna, P., Taviani, M., Falter, J., Thresher, R., Hosie, A., Haig, D., Foglini, F., Hua, Q., and McCulloch, M. T. (2019). First ROV exploration of the Perth Canyon: Canyon setting, faunal observations, and anthropogenic impacts. Frontiers in Marine Science, 6, 173. https://doi.org/10.3389/fmars.2019.00173

Veatch, J. M., Kohut, J. T., Oliver, M. J., Statscewich, H., and Fredj, E. (2024). Quantifying the role of submesoscale Lagrangian transport features in the concentration of phytoplankton in a coastal system. ICES Journal of Marine Science, 81(4), 760-773.

Verspecht, F., and Pattiaratchi, C. (2010). On the significance of wind event frequency for particulate resuspension and light attenuation in coastal waters. Continental Shelf Research, 30(18), 1971-1982. https://doi.org/10.1016/j.csr.2010.09.008

Waite, A.M.; Thompson, P.A.; Pesant, S.; Feng, M.; Beckley, L.E.; Domingues, C.M.; Gaughan, D.; Hanson, C.E.; Holl, C.M.; Koslow, T and Twomey, L. (2007). The Leeuwin Current and its eddies: An introductory overview. Deep Sea Research Part II: Topical Studies in Oceanography, 54(8-10), 789-796. https://doi.org/10.1016/j.dsr2.2006.12.008

Wijeratne, S., Pattiaratchi, C., and Proctor, R. (2018). Estimates of surface and subsurface boundary current transport around Australia. Journal of Geophysical Research: Oceans, 123(5), 3444-3466. https://doi.org/10.1029/2017JC013221

Woo, L. M. (2021). Delayed Mode QA/QC Best Practice Manual (https://content.aodn.org.au/Documents/IMOS/Facilities/Ocean_glider/Delayed_Mode_QAQC_Best_Practice_Manual_OceanGliders_v3.0.pdf).

Zaker, N. H., Imberger, J., and Pattiaratchi, C. (2007). Dynamics of the coastal boundary layer off Perth, Western Australia. Journal of Coastal Research, 23(5), 1112-1130. https://doi.org/10.2112/04-0374.1

Zatsepin, A., Kubryakov, A., Aleskerova, A., Elkin, D., & Kukleva, O. (2019). Physical mechanisms of submesoscale eddies generation: evidences from laboratory modeling and satellite data in the Black Sea. Ocean dynamics, 69, 253-266.

Zhang, Y., Hu, C., Liu, Y., Weisberg, R. H., & Kourafalou, V. H. (2019). Submesoscale and mesoscale eddies in the Florida Straits: Observations from satellite ocean color measurements. Geophysical Research Letters, 46(22), 13262-13270.

Zhang, Z., & Qiu, B. (2020). Surface chlorophyll enhancement in mesoscale eddies by submesoscale spiral bands. Geophysical Research Letters, 47(14), e2020GL088820.

Zhang, Y., & Tian, J. (2014). Enhanced turbulent mixing induced by strong wind on the South China Sea shelf. Ocean Dynamics, 64(6), 781-796.

Zhu, Y., Li, Y., Yang, Y., & Wang, F. (2023). The role of eddy-wind interaction in the eddy kinetic energy budget of the Agulhas retroflection region. Environmental Research Letters, 18(10), 104032.